AFIT/GAE/ENY/91D-16

(1)

COMPARISON OF POINTING CONTROL SYSTEMS UTILIZING DAHL AND COULOMB FRICTION MODEL COMPENSATION

THESIS

Whitney J. Hulett, Captain, USAF

AFIT/GAE/ENY/91D-16

Approved for public release; distribution unlimited

AFIT/GAE/ENY/91D-16

COMPARISON OF POINTING CONTROL SYSTEMS UTILIZING DAHL AND COULOMB FRICTION COMPENSATION

THESIS

Presented to the Faculty of the School of Engineering

of the Air Force Institute of Technology

Air University

In Partial Fulfillment of the

Requirements for the Degree of

Master of Science in Aeronautical Engineering

Whitney J. Hulett, B.S.

Captain, USAF

December 1991

Acknowledgments

Even though this thesis does not present any earth shattering conclusions about the physical universe as we know it, there is one person who will read this thesis, and his eyes will light up and his face will beam with pride--and even though he doesn't understand half of what he has read, to him it will be as if I had solved all of the world's problems. I would like to dedicate this thesis, and all of the hard work and effort that was put into it, to my biggest fan, my worst critic, my hardest teacher, and my best friend...my father. Thank you.

Whitney Jonas Hulett

Table of Contents

List of Figures

List of Symbols

Deg	Degree
Sec	Second
T_c	Running Friction Torque
T_F	Friction Torque
T_m	Motor Torque
J	Moment of Inertia
θ	Deflection Angle
θ_c	Commanded Input Deflection
$\dot{\theta}$	Gimbal Rate
$\ddot{\theta}$	Acceleration
σ	Dahl Friction Model Rest Slope Parameter
i	Dahl Friction Model Exponential Parameter
x_c	Dahl Friction Compliance Zone
Q	Covariance of the System Noise
R	Covariance of the Measurement Noise
k	Regulator Gains
L	Estimator Gains

Abstract

Bearing friction can be accurately modeled using the Coulomb friction model, provided the bearing is running. In an application where the bearing is rotated only a very small amount, the bearing does not actually rotate. Instead, the bearing undergoes *plastic* deformation. A nonlinear friction model was developed by P. R. Dahl of the Aerospace Corporation in the late sixties which addresses this region of placticity or compliance zone. Two friction compensation schemes for a single axis position servomechanism were developed and compared in this study. The first compensator was an integral control regulator/estimator which used the Coulomb friction model. The second, more complicated compensator, was an extended Kalman filter (EKF) design which used the Dahl friction model. The compensator designs were simulated using ProMatlab™. Comparisons were made of the time response characteristics to determine if any increases in performance were worth the added complexity of the Dahl model EKF controller.

COMPARISON OF POINTING CONTROL SYSTEMS UTILIZING DAHL AND COULOMB FRICTION MODEL COMPENSATION

I. Introduction and Background

1.1 Problem Motivation

As technology increases, so does the demand on control systems. New weapon systems, such as those proposed under the umbrella of the Strategic Defense Initiative, will require servomechanism pointing control to accuracies down to the milli-radian and even micro-radian level. Precision pointing control of any gimballed object is hampered by many nonlinear disturbance forces or torques. These may include cogging torques, magnetic drag torques, resistant forces caused by the restricted range of motion of cables or wire harnesses, and of course, the frictional torques caused by the contacting surfaces of the bearings. These frictional torques affect the precision pointing capabilities the most.

Since the dawn of time, mankind has had to deal with the good and bad aspects of friction. If it weren't for friction, our ancestors would not have been able to rub two sticks together to make the fires essential to their survival. In fact, if it weren't for friction, the simplest tasks such as walking

would be impossible as we know it. Yet a vast majority of the scientific community will neglect the effects of friction where at all possible, because of the added complexity involved when friction is retained. In his doctoral dissertation, Brian Armstrong commented on something Leonardo da Vinci wrote a long time ago concerning the lack of friction among the planets and stars.

> Leonardo understood that the friction is absent from the state of grace. Thus friction is confined to this mortal world: friction is a consequence of original sin...But for all of this, in the discussion of dynamics for control of mechanical systems friction is but little studied and often omitted. (1:1)

Even when we do address friction, we usually do so in such a simplified, cursory fashion that it often taints the physical essence of the design work.

When friction is accounted for, the question of which friction model to use must still be answered. There are several friction models of varying complexity which may offer the designer varying levels of performance over the entire spectrum of the friction regime. There also exists, within the realm of friction, different regions of interest. The physics of these different regions may vary substantually, such that they absolutely require different models to represent them accurately.

Two friction models that are of interest for this thesis are the Coulomb friction model and the Dahl friction model. The Coulomb, or running friction model as it is often called, was developed by Charles Augustin Coulomb around the year 1781. In the simpler running friction model, Coulomb

proposed the existance of a constant force which acted against, or with, the external force depending on the direction of the velocity. The Dahl model, developed by P.R. Dahl in 1969, treats friction as a nonlinear spring or elastic region for small deflections while for large deflections the friction value approaches the running or Coulomb friction value. Both of these will be discussed in much greater detail in Chapter Two and Chapter Three.

1.2 Previous Work

Tribology, the study of wear and friction, has existed for many hundreds of years. There has, however, only been a moderate amount of work done on adaptive friction compensation, with the majority in just the past five to ten years. Still, several articles have been published on this particular topic. There are two papers that relate closely to this research effort. One was written by Lewis C. Himmel, et. al., of The Aerospace Co. (2:642-643) and the other was written by Craig D. Walrath of the Westinghouse Defense and Electronics Center (3:721-722).

Both papers examine the use of adaptive control techniques for friction compensation, and both utilize the Dahl friction model. The papers differ in the estimation techniques for the adaptive control. Himmel and company used a second order difference scheme to estimate the friction acceleration. Walrath, on the other hand, developed an adaptive filter which used a scaled bilinear transformation to estimate the Dahl friction parameters. Block

diagrams for the two schemes are shown in Figures 1-1 and 1-2.

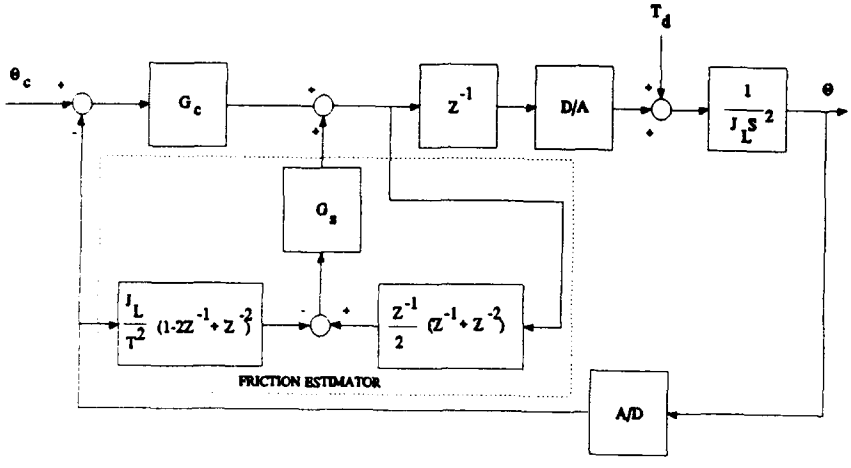

Figure 1-1 Mathematical Model for the Himmell Friction Compensator.

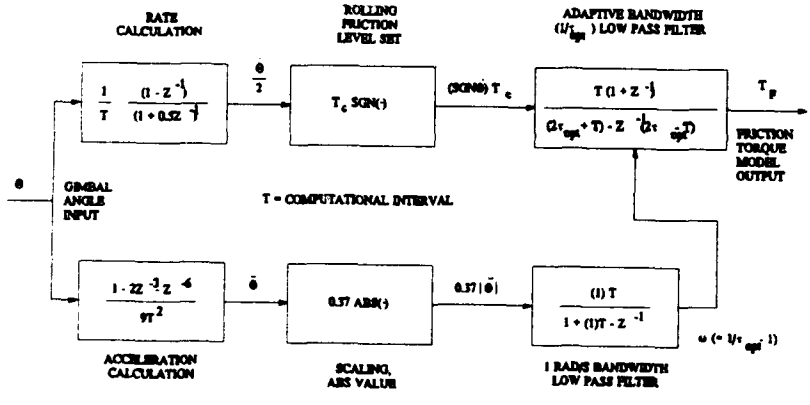

Figure 1-2 Mathematical Model of the Walrath Friction Compensator.

1.3 Present Work

In this research, friction compensators were designed for a single axis position servomechanism using both the Coulomb friction model and the more complex Dahl friction model. Two compensators were designed using position feedback only. The first design used the Coulomb friction model and incorporated integral control action in a regulator/estimator in an attempt to cancel the actual friction prior to entering the plant model. The second compensation scheme used the more complicated Dahl friction model along with an Extended Kalman Filter (EKF) to provide adaptive control techniques in estimating the Dahl friction parameters. This compensator design also attempted to estimate and cancel the friction prior to the plant process. These designs were then simulated using ProMatlab™. Simulations were done using both large and small magnitude commanded inputs. This was to insure that both the elastic friction region, for small deflections, as well as the running friction region, for large deflections, were covered in the investigation. One of the main focal points of this research was to determine whether the advantages of using the Dahl model EKF friction compensator outweigh the obvious disadvantages in design complexity and large onboard computing power that is required.

II. Friction Theory

2.1 Coulomb Friction

Ordinary, common, everyday friction can be divided into two parts: static friction and dynamic friction. Static friction, or *stiction* as it is sometimes called, refers to the friction force of a static system, which must be overcome in order for the system to move. Dynamic friction refers to the frictional force of the dynamic system once the motion has begun. The force required to overcome the static friction force is greater than the force

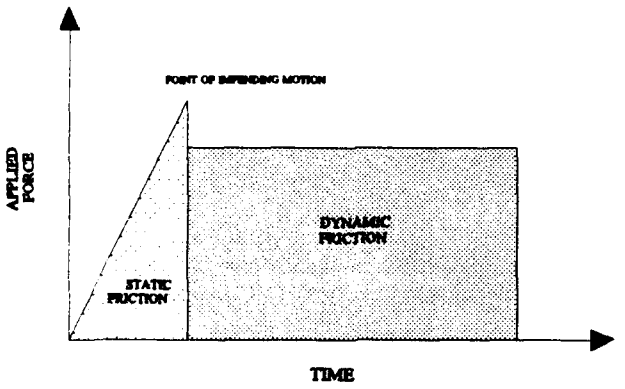

Figure 2-1 Plot of Ideal Friction vs Time

required to keep it moving. Figure 2-1 shows this phenomenon graphically (4:251). A good physical example (one that most everyone is probably

familiar with) might be the graduating AFIT student, packing their belongings to move on the next challenge. Inevitably they will pack all of their text books into one big box. Because this box is so heavy, the only way to move it is to slide it across the floor. The student begins pushing the box but it doesn't move. The student pushes steadily harder until suddenly the force applied by the student overcomes the *stiction* force and the box begins to slide across the floor. However, once the box has begun moving, the student notices that a smaller force is required to keep the box moving at the same velocity. The point where the applied force was equal to the static friction force is known as the point of *impending motion* or *impending slippage* (4:251).

In the year 1781, Charles Augustin Coulomb conducted experiments with sliding blocks. He made three conclusions which are applicable at or after the point of impending motion. These conclusions are:

1. The total force of friction that can be developed is independent of the magnitude of the area of contact.

2. For low relative velocities between sliding objects, the frictional force is practically independent of velocity. However, the sliding frictional force is less than the frictional force corresponding to impending slippage.

3. The total frictional force that can be developed is proportional to the normal force transmitted across the surface of contact. (4:252)

Today, these conclusions are known as Coulomb's laws of friction. Furthermore, because Coulomb's laws apply to the dynamic friction region,

Coulomb friction is often referred to as *running* friction.

2.2 Dahl Friction

The Dahl friction model was developed by P. R. Dahl in the late sixties as a new math model for solid friction. Over the years it has gained acceptance by the scientific and engineering community, mainly as a ball bearing friction model, which fits in well with this research.

Dahl made the observation that the time rate of change of solid friction could be expressed as

$$\frac{dF(x,t)}{dt} = \frac{dF(x)}{dx}\frac{dx}{dt} \tag{2.1}$$

where F(x) is the solid friction force as a function of the relative displacement, x. Dahl claims that the typical friction force, F(x), is like that shown in Figure 2-2. Here you can see that the friction force monotonically

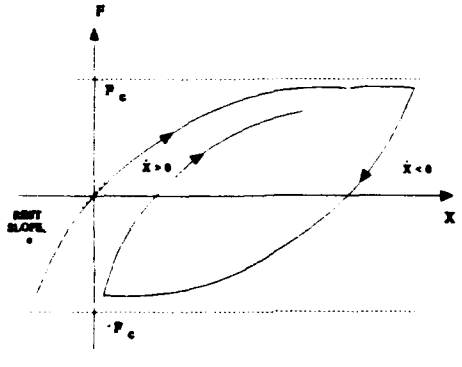

Figure 2-2 Typical Dahl Friction Force Function

approaches $\pm F_c$, which is the running friction value, depending on the direction of the velocity. For $\dot{x} > 0$, F(x) approaches $+F_c$ and for $\dot{x} < 0$, F(x) approaches $-F_c$. Notice that in Figure 2-2 the friction function slope, $\frac{dF(x)}{dx}$, remains positive, even when the direction of the rate, $\dot{x}$, changes. Dahl experimentally determined this friction slope function, $\frac{dF(x)}{dx}$, to be described by

$$\frac{dF(x)}{dx} = \sigma \left| 1 - \frac{F}{F_c} sgn\dot{x} \right|^i \tag{2.2}$$

where: σ = Rest stiffness parameter
F_c = Coulomb or running friction parameter
i = Solid friction exponent parameter

The Dahl friction model, in essence, behaves like a *soft* spring for small deflection, yet approaches the Coulomb friction value for large deflections. Physically what this means, when applied to a ball bearing, is that the bearing will deform slightly before it begins to roll. If the deflection is small enough, the bearing may never roll at all--just experience plastic deformation. This region in which the bearing deforms is the elastic region, which Dahl says behaves like a nonlinear spring. From this point on, this elastic region will be referred to as the *compliance zone*. This compliance zone is essentially neglected by the Coulomb model. In using the Coulomb friction model, the assumption is usually made that the magnitude of the relative deflection is greater than the compliance zone, thereby jumping immediately to the running

friction value.

The reader might also have noticed that, according to the Dahl model (see Figure 2-3), the friction value, F, is never greater than the running friction value, F_c. This is contrary to what Coulomb postulated (recall Figure 2-1) when he observed a stiction value larger than the running friction at the point of impending motion. Dahl (5:53-56) and others (6:24) have conducted numerous experiments in this area and have concluded that, for ball bearing friction at least, the breakaway friction value is not greater than the running friction.

Integrating equation 2.2 with respect to x (with F(0)=0) yields

$$\frac{F}{F_c} = 1 - [\,1 - (1-i)\frac{x}{x_c}\,]^{\frac{1}{(1-i)}} \qquad (2.3)$$

for $i \neq 1$, and

$$\frac{F}{F_c} = (\,1 - e^{-\frac{x}{x_c}}\,) \qquad (2.4)$$

for $i = 1$, where

$$x_c = \frac{F_c}{\sigma} \qquad (2.5)$$

The force deflection loops (equation 2.3) for i=0, i=¼, i=½, i=1, and i=2 are plotted in Figure 2-3 (7:3). It should be easy to see here the physical significance of x_c. It is the *knee* of the force deflection curve, or the

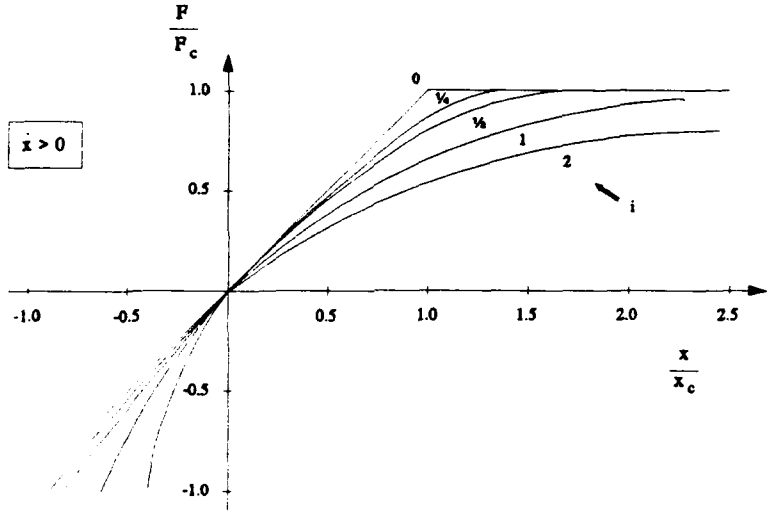

Figure 2-3 Force Deflection Curves for Varying i

point where the model essentially changes from a nonlinear elastic spring to a more conventional Coulomb friction model. Thus, the compliance zone can be estimated using equation 2.5.

III. Compensator Designs

3.1 The Single Axis System and Assumptions

3.1.1 The Single Axis System. As mentioned previously, the system that was used for this study was a single axis servomechanism or gimbal. Consider a system like the one shown in Figure 3-1 limited to a single degree of freedom. For the purposes of this study, it was assumed that the motor torque and rotation were in the same direction, and the friction torque was

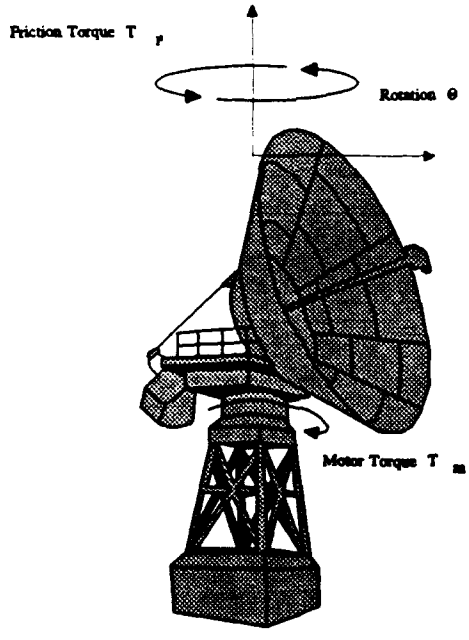

Figure 3-1 Single Axis Servo Reference Frame

opposing the motor torque. The equation of motion for this system is

$$J\,\ddot{\Theta} = T_m - T_F \tag{3.1}$$

where J = moment of inertia for the system
T_m = motor torque
T_F = friction torque

Equation 3.1 can be rewritten as

$$\ddot{\Theta} = \frac{1}{J}(T_m - T_F) \tag{3.2}$$

If we neglect the friction and set $T_F = 0$, a state space representation of the system would be

$$\dot{x} = \begin{bmatrix} 0 & 1 \\ 0 & 0 \end{bmatrix} x + \begin{bmatrix} 0 \\ \frac{1}{J} \end{bmatrix} u \tag{3.3}$$

$$y = [1 \;\; 0]\, x$$

where the state and the input are

$$x = \begin{bmatrix} \theta \\ \dot{\theta} \end{bmatrix} \quad ; \quad u = T_m$$

A block diagram of this simplified system is shown in figure 3-2.

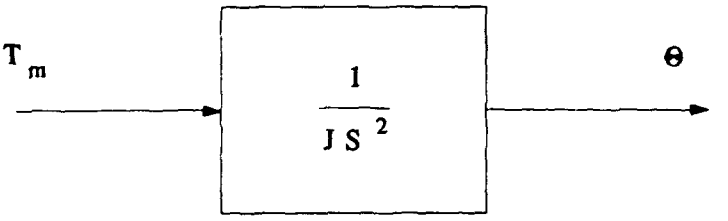

Figure 3-2 Block Diagram of Simplified Servo

3.1.2 Assumptions. Since we are interested in the effects of friction in this study, T_F cannot be neglected. Additionally, for us to design and simulate controllers that cancel out the effects of friction, the actual friction must be known, or a friction model must be chosen to represent the true friction. It has been shown by Dahl and others that the Dahl model is an accurate representation of the actual bearing friction (5:53-60), (7:24). Therefore, it was assumed here that the Dahl friction parameters σ, i, and T_c (the running friction torque) were known for the true friction. Using this as the truth model, compensators could then be designed to cancel the friction.

A block diagram of this general system without the feedback controller is shown in Figure 3-3. In addition, it was assumed that the moment of inertia, J, was known and constant with time.

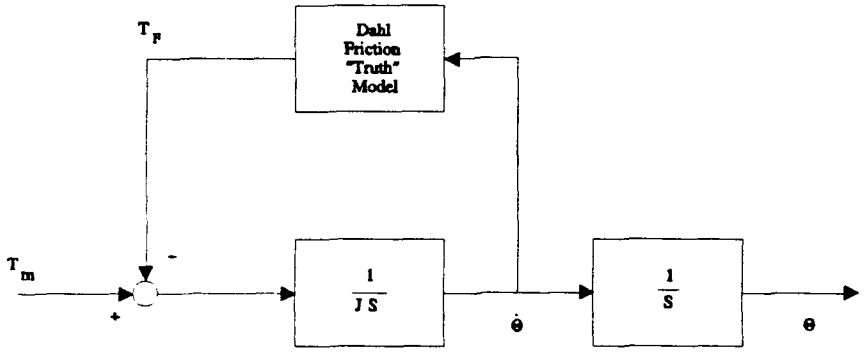

Figure 3-3 System with Friction Truth Model

Equation 3.4 is the state space representation of the system with the Dahl model imposed as the true friction model.

$$\dot{x} = \begin{bmatrix} 0 & 1 & 0 \\ 0 & 0 & -\frac{1}{J} \\ 0 & DF & 0 \end{bmatrix} x + \begin{bmatrix} 0 \\ \frac{1}{J} \\ 0 \end{bmatrix} u \qquad (3.4)$$

$$y = [1 \ 0 \ 0]x$$

where

$$x = \begin{bmatrix} \theta \\ \dot{\theta} \\ T_F \end{bmatrix} \quad ; \quad u = T_m$$

and

$$DF = \sigma \left| 1 - \frac{T}{T_c} sgn\dot{\theta} \right|^i$$

which is the Dahl friction model.

3.2 Integral Action Regulator/Estimator with Coulomb Friction

3.2.1 Integral Action. It is very desirable to have zero steady state error in a precision pointing application. To accomplish this, integral control action was employed. Integral control was introduced by augmenting the state vector with the desired integration, which in this case was the friction torque, T_F (8:387). The compensator state vector became

$$x = \begin{bmatrix} \theta \\ \dot{\theta} \\ T_F \end{bmatrix}$$

which will work nicely with the Coulomb friction model. This will be shown later.

3.2.2 The Coulomb Regulator/Estimator. The following sections describe the technique used to design the friction compensator using the Coulomb friction model and regulator and estimator theory.

3.2.2.1 State Space Representation with Integral Action. In dynamical systems, Coulomb friction is often modelled as a piece-wise linear function similar to that shown in Figure 3-4. The friction value is instantaniously set to positive running friction value for positive velocities and to negative running friction value for negative velocities. Intuitively,the friction value would then be equal to zero for zero velocity.

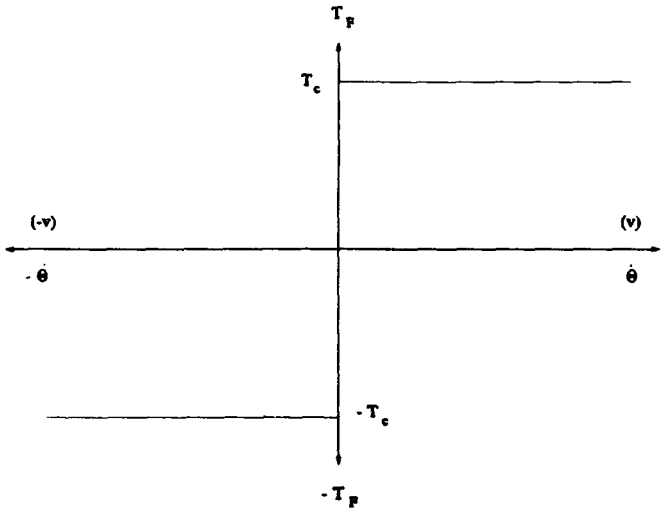

Figure 3-4 Coulomb Friction Model

Clearly, in this friction model, the friction torque does not change with velocity (i.e. $\frac{dT_F}{dv} = 0$) except at the discontinuity point, where the velocity

is zero. It can also be said that the friction torque does not change with time since

$$\frac{dT_F}{dt} = \frac{dT_F}{dv}\frac{dv}{dt} \tag{3.5}$$

and

$$\frac{dT_F}{dv} = 0$$

This works well given our desire to implement integral action. By augmenting the state vector with T_F, $\dot{T}_F$ (which is $\frac{dT_F}{dt}$) was required to form the state space representation. The state space equation for the integral augmented system with the Coulomb friction model is then

$$\dot{\boldsymbol{x}} = \boldsymbol{A}\boldsymbol{x} + \boldsymbol{B}\boldsymbol{u}$$

$$y = \boldsymbol{C}\boldsymbol{x}$$

or

$$\dot{\boldsymbol{x}} = \begin{bmatrix} 0 & 1 & 0 \\ 0 & 0 & -\frac{1}{J} \\ 0 & 0 & 0 \end{bmatrix} \boldsymbol{x} + \begin{bmatrix} 0 \\ \frac{1}{J} \\ 0 \end{bmatrix} u \tag{3.6}$$

$$y = [1 \;\; 0 \;\; 0]\, x$$

where

$$\dot{x} = \begin{bmatrix} \theta \\ \dot{\theta} \\ T_F \end{bmatrix} \quad ; \quad u = T_m$$

The augmented A matrix in equation 3.6 has one complete row of zeroes which represents a pole at the origin; or a pure integrator.

3.2.2.2 The Regulator/Estimator Problem. For the system

$$\dot{x} = Ax + Bu$$

$$y = Cx$$

recall that the Luenberger estimator is

$$\dot{\hat{x}} = A\hat{x} + Bu + L(y - C\hat{x}) \tag{3.7}$$

where $\hat{x}$ is the estimate of the state and **L** is the proportional estimator gain matrix, chosen to achieve satisfactory error characteristics (8:345). Combining like terms in equation 3.7 yields

$$\dot{\hat{x}} = (A-LC)\hat{x} + Bu + Ly \tag{3.8}$$

For the regulator, we combine equation 3.8 with the control law

$$u = -k\hat{x} \tag{3.9}$$

and assuming there is no command input, we get

$$\dot{\hat{x}} = (A-LC)\hat{x} + B(-k\hat{x}) + Ly \tag{3.10}$$

or

$$\dot{\hat{x}} = (A-Bk-LC)\hat{x} + Ly \tag{3.11}$$

where k is the proportional regulator gain marix. Substituting y=Cx into equation 3.11, we get

$$\dot{\hat{x}} = (A-Bk-LC)\hat{x} + L(Cx) \tag{3.12}$$

or

$$\dot{\hat{x}} = \tilde{A}\hat{x} + \tilde{B}\tilde{u} \tag{3.13}$$

where

$$\tilde{A} = A - Bk - LC \quad ; \quad \tilde{B} = L \quad and \quad \tilde{u} = Cx$$

For the servo model that was generated earlier, y=Cx or

$$y = \begin{bmatrix} 1 & 0 & 0 \end{bmatrix} \begin{bmatrix} \Theta \\ \dot{\Theta} \\ T_F \end{bmatrix} = \Theta$$

Therefore, according to equation 3.13, the input to the regulator, u, should be Θ. But that was for a system with no commanded input. However, since we wish to perform a command following task, we need to difference Θ with a command input, Θ_c. Thus, equation 3.7 becomes

$$\dot{\hat{x}} = A\hat{x} + Bu + L(y - C\hat{x} - \Theta_c) \tag{3.7a}$$

Following the same procedures as before yields

$$\dot{\hat{x}} = (A - Bk - LC)\hat{x} + L(Cx - \Theta_c) \tag{3.12a}$$

and since Cx=Θ

$$\dot{\hat{x}} = (A - Bk - LC)\hat{x} + L(\Theta - \Theta_c) \tag{3.12b}$$

This effectively provides error feedback for command following type systems (9). The block diagram of the system developed so far is shown in Figure 3-5.

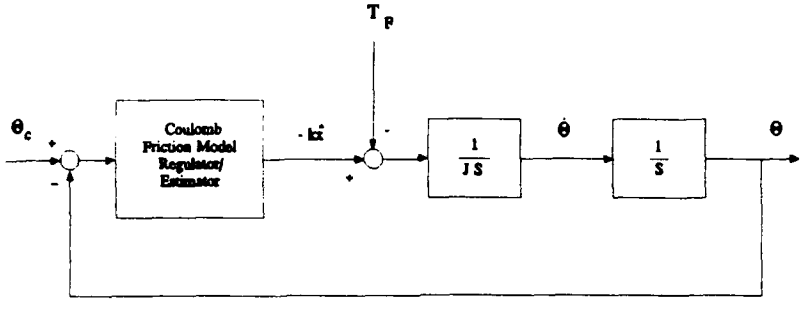

Figure 3-5 Coulomb Friction Model Reg/Est Compensator

3.2.2.3 ***Incorporation of the "True" Friction.*** Combining the results of the last section with the true friction model assumptions made in Section 3.1.2 yields the system shown in Figure 3-6. As was mentioned in the introduction, the objective of the compensator is to cancel out the friction.

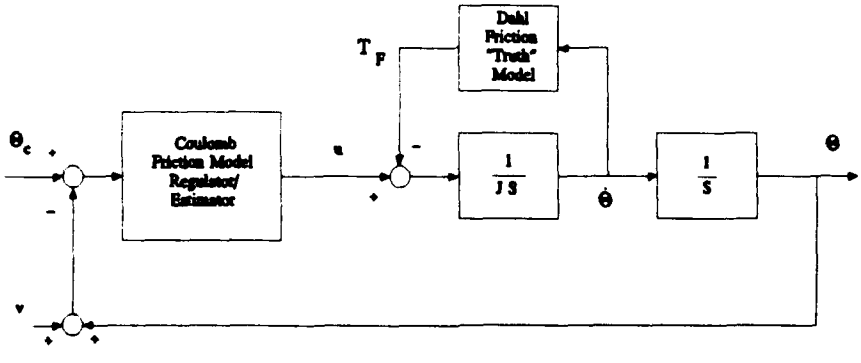

Figure 3-6 Coulomb Compensator with True Friction

To accomplish this, u, which is $-\mathbf{k}\hat{\mathbf{x}}$, would have to contain the estimate of friction, $\hat{T}_F$. This was accomplished by the following method. The regulator gains, $\mathbf{k}=[k_1,k_2,k_3]$, and the estimator gains, $\mathbf{L}=[l_1,l_2,l_3]^T$, were determined by placing the regulator and estimator poles with full state feedback to get the desired transient response and error characteristics. This was done using the *Place* command in ProMatlab™, which uses a technique described in a report by Kautsky and Nichols on robust eigenstructure assignment in state feedback control (10). The regulator poles were only placed for the 2-state plant, $\frac{1}{JS^2}$. This gave values for k_1 and k_2, but since the goal was to try to cancel friction, k_3 is set to -1. Thus,

$$u = -k\hat{x} = -\begin{bmatrix} k_1 & k_2 & -1 \end{bmatrix} \begin{bmatrix} \hat{\theta} \\ \dot{\hat{\theta}} \\ \hat{T}_F \end{bmatrix}$$

or

$$u = -k_1\hat{\theta} - k_2\dot{\hat{\theta}} + \hat{T}_F \tag{3.14}$$

The entire state space equation is then

$$\dot{x} = \begin{bmatrix} \dot{\theta} \\ \ddot{\theta} \\ \dot{T}_F \end{bmatrix} = \begin{bmatrix} 0 & 1 & 0 \\ 0 & 0 & -\frac{1}{J} \\ 0 & DF & 0 \end{bmatrix} \begin{bmatrix} \theta \\ \dot{\theta} \\ T_F \end{bmatrix} + \begin{bmatrix} 0 \\ \frac{1}{J} \\ 0 \end{bmatrix} \left[-k_1\hat{\theta} - k_2\dot{\hat{\theta}} + \hat{T}_F \right] \tag{3.15}$$

From equation 3.15, we can extract $\ddot{\theta}$, which is

$$\ddot{\theta} = \frac{1}{J} \left[-T_F - k_1\hat{\theta} - k_2\dot{\hat{\theta}} + \hat{T}_F \right] \tag{3.16}$$

It should be easy to see from equation 3.16 that with a good job of estimating the friction torque (i.e. $T_F \approx \hat{T}_F$) the compensator should cancel out the true friction torque resulting in a seemingly frictionless system. This should give better response characteristics for both large and small deflections.

Notice also, that in Figure 3-6, sensor noise (v) can inserted into the system model.

3.3 Extended Kalman Filter with Dahl Friction Model

This section covers the development of the extended Kalman filter friction compensator. The basic theory of the extended Kalman filter is discussed first, followed by the specific application to this problem.

3.3.1 Extended Kalman Filter Theory. The extended Kalman filter (EKF) is used in nonlinear system applications where the linearized filter

breaks down. The basic principle of the EKF is to relinearize about each estimate of the state, $\hat{x}$, after it is computed. After each consecutive time step, t_i^+, the state vector, $x(t_i^+)$ is recomputed and a new estimate of the state trajectory is made (11:42). This assumes that the step size is sufficiently small such that the linearization is a good approximation of the nonlinear state equation.

In general, the state space equations are

$$\begin{aligned} \dot{x} &= f(x,u,t) + G(t)w(t) \\ z &= h(x,t) + v(t) \end{aligned} \tag{3.17}$$

where
- $\mathbf{x}$ is the state vector
- $\mathbf{f}(\mathbf{x},\mathbf{u},t)$ is some nonlinear function of $\mathbf{x}(t)$, $\mathbf{u}(t)$, and t
- $\mathbf{z}$ is the measurement which may be a nonlinear function of $\mathbf{x}$ and t
- $\mathbf{v},\mathbf{w}$ are uncorrelated, zero-mean, white gaussian noise vectors with $E\{\mathbf{w}(t)\mathbf{w}^T(t-\tau)\}=\mathbf{Q}(t)\delta(t-\tau)$ and $E\{\mathbf{v}(t)\mathbf{v}^T(t-\tau)\}=\mathbf{R}(t)\delta(t-\tau)$

The EKF updates the measurement, $\mathbf{z}_i$, through the folowing equations

$$K(t_i) = P(t_i^-)H^T\left[t_i;\hat{x}(t_i^-)\right]\left(H\left[t_i;\hat{x}(t_i^-)\right]P(t_i^-)H^T\left[t_i;\hat{x}(t_i^-)\right] + R(t_i)\right)^{-1} \tag{3.18}$$

$$\hat{x}(t_i^+) = \hat{x}(t_i^-) + K(t_i)\left(z(t_i) - H\left[\hat{x}(t_i^-),t_i\right]\right) \tag{3.19}$$

$$P(t_i^+) = P(t_i^-) - K(t_i)H\left[t_i;\hat{x}(t_i^-)\right]P(t_i^-) \tag{3.20}$$

where

$$H\left[t_i;\hat{x}(t_i^-)\right] \triangleq \left.\frac{\partial h[x,t_i]}{\partial x}\right|_{x=\hat{x}(t_i^-)}$$

The estimate is propagated forward in time to the next sample t_{i+1} by integrating the following equations from time t_i to t_{i+1}:

$$\dot{\hat{x}}\,(t/t_i) = f\left[\hat{x}(t/t_i),u(t),t\right] \tag{3.21}$$

$$\dot{P}(t/t_i) = F\left[t;\hat{x}(t/t_i)\right]P(t/t_i) + P(t/t_i)F^T\left[t;\hat{x}(t/t_i)\right] + G(t)Q(t)G^T(t) \tag{3.22}$$

where

$$F\left[t;\hat{x}(t/t_i)\right] \triangleq \left.\frac{\partial f[x,u,t]}{\partial x}\right|_{x=\hat{x}(t/t_i)}$$

(11:44-45).

3.3.2 EKF Applied to the Single Axis Servo. Recall the Dahl friction model

$$\dot{T}_F = DF\,\dot{\Theta}$$

where

$$DF = \sigma \left| 1 - \frac{T}{T_c} sgn\dot{\Theta} \right|^i$$

In order for the friction to be estimated we must also estimate the Dahl friction parameters, σ, i, and T_c. It will be assumed here that the running friction value, T_c, can be measured a priori and only σ and i need to be estimated. Therfore, σ and i were added to the state. Thus,

$$x = \begin{bmatrix} \Theta \\ \dot{\Theta} \\ T_F \\ \sigma \\ i \end{bmatrix} \tag{3.23}$$

Since σ and i are constants, their time derivatives are equal to zero. Therefore, the state space equation becomes

$$\dot{x} = f(x,u,t) = \begin{bmatrix} \dot{\Theta} \\ \ddot{\Theta} \\ \dot{T}_F \\ \dot{\sigma} \\ \dot{i} \end{bmatrix} = \begin{bmatrix} \dot{\Theta} \\ \frac{1}{J}(u - T_F) \\ \sigma \left[1 - \frac{T_F}{T_c} sgn\dot{\Theta} \right]^i \dot{\Theta} \\ 0 \\ 0 \end{bmatrix} \tag{3.24}$$

$$z = hx = \begin{bmatrix} 1 & 0 & 0 & 0 & 0 \end{bmatrix} \begin{bmatrix} \Theta \\ \dot{\Theta} \\ T_F \\ \sigma \\ i \end{bmatrix} = \Theta$$

Solving for the Jacobian, **F**[t;**x**], we get

$$\frac{\partial f}{\partial x} = \begin{bmatrix} \frac{\partial f}{\partial \Theta} & \frac{\partial f}{\partial \dot{\Theta}} & \frac{\partial f}{\partial T_F} & \frac{\partial f}{\partial \sigma} & \frac{\partial f}{\partial i} \end{bmatrix}$$

where

$$\frac{\partial f}{\partial \Theta} = \begin{bmatrix} 0 \\ 0 \\ 0 \\ 0 \\ 0 \end{bmatrix}$$

$$\frac{\partial f}{\partial \dot{\Theta}} = \begin{bmatrix} 1 \\ 0 \\ \sigma \left[1 - \frac{T_F}{T_c} sgn\, \dot{\Theta} \right] i \\ 0 \\ 0 \end{bmatrix}$$

$$\frac{\partial f}{\partial T_F} = \begin{bmatrix} 0 \\ -\frac{1}{J} \\ \sigma\, i \left[1 - \frac{T_F}{T_c} sgn\,\dot{\Theta}\right]^{i-1} \dot{\Theta} \left(-\frac{1}{T_c} sgn\,\dot{\Theta}\right) \\ 0 \\ 0 \end{bmatrix}$$

$$\frac{\partial f}{\partial \sigma} = \begin{bmatrix} 0 \\ 0 \\ \left[1 - \frac{T_F}{T_c} sgn\,\dot{\Theta}\right]^{i} \dot{\Theta} \\ 0 \\ 0 \end{bmatrix}$$

$$\frac{\partial f}{\partial i} = \begin{bmatrix} 0 \\ 0 \\ \sigma \left[1 - \frac{T_F}{T_c} sgn\,\dot{\Theta}\right]^{i} \dot{\Theta} \ln \left(1 - \frac{T_F}{T_c} sgn\,\dot{\Theta}\right) \\ 0 \\ 0 \end{bmatrix}$$

Similarly,

$$\boldsymbol{H} = \begin{bmatrix} \frac{\partial h}{\partial \Theta} & \frac{\partial h}{\partial \dot{\Theta}} & \frac{\partial h}{\partial T_F} & \frac{\partial h}{\partial \sigma} & \frac{\partial h}{\partial i} \end{bmatrix}$$

or

$$H = [1\ 0\ 0\ 0\ 0]$$

for this problem.

Now we can combine the results from the previous sections concerning the EKF Dahl compensator. The complete system is shown in figure 3-7.

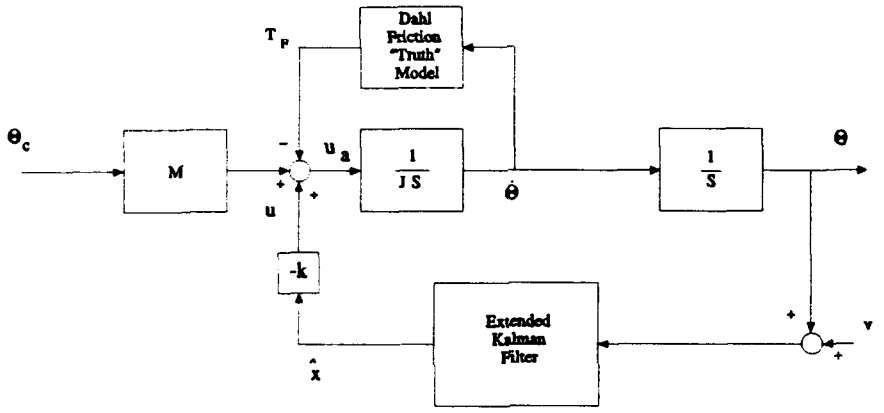

Figure 3-7 Single Axis System with EKF Compensator

As was the case with the Coulomb model regulator/estimator, we are introducing an estimate of the state, $\hat{x}$. This state estimate contains an estimate of the friction value, $\hat{T}_F$, which is summed with the actual friction, T_F , prior to entering the plant process. Here again, it should be clear to see that if we do a good job estimating $\hat{T}_F$, it will cancel the actual friction and the system will act as thought it were frictionless.

One particular subtlety that has not been discussed is the proportional gain matrix **M** that pre-multiplies the commanded input, u_c or Θ_c. This is done for a command following system to insure that the steady state solution is equal to the input or $\Theta_{ss} = \Theta_c$. M is calculated in the following manner. The system under consideration is

$$\dot{x} = Ax + Bu$$

$$y = Cx$$

$$u = -kx + My_c$$

where, for this example, $y=\Theta$ and $y_c=\Theta_c$. In the steady state, $\hat{x}\rightarrow x$ and $\dot{x}\rightarrow 0$. Thus we get

$$0 = Ax_{ss} + Bu_{ss} \tag{3.25}$$

$$y_{ss} = Cx_{ss} \tag{3.26}$$

$$u_{ss} = -kx_{ss} + My_c \tag{3.27}$$

Solving equations 3.25 through 3.27 for y_{ss} yields

$$y_{ss} = C[Bk - A]^{-1}BMy_c \tag{3.28}$$

Requiring that $y_{ss}=y_c$, we can solve directly for **M** which is

$$M = \left(C[Bk - A]^{-1}B\right)^{-1} \tag{3.29}$$

3.4 Simulation of the Compensator Designs

The following section discusses the manner in which the single axis servo system was dynamically simulated with each friction model compensator. Both compensators were simulated using ProMatlab™ on the AFIT Vax mainframe computer known as *Hercules*. ProMatlab™ is a matrix manipulation and control system design software package developed by Mathworks. It is assumed that the reader has some working knowledge of these types of programs. Therefore, the exact workings of ProMatlab™ will not be discussed in this thesis except where required to adequately explain the procedure or results.

3.4.1 Coulomb Model Compensator Simulation. The single axis system with a Coulomb friction model compensator developed in section 3.2 (see Figure 3-6) was coded into two ProMatlab™ macros or m-files. The exact code for the two macros (*Coulomb1.m* and *Coulomb2.m*) that was used for these simulations is shown in Appendix A.

3.4.1.1 Coulomb1.m. The logic of the first macro, *Coulomb1.m*, closely parallels the development in Section 3.2.2. As mentioned previously in that section, the regulator and estimator gains, **k** and **L** must be available in the variable list for *Coulomb1.m* to use. The following is the basic logic of the macro. *Coulomb1.m* takes the gains **k** and **L** and calculates the closed-loop regulator/estimator compensator state space **A** and **B** matrices. These are then discretized using the ProMatlab™ *C2D* (continuous to discrete) command. The technique used in ProMatlab™ to discretize these matrices is

$$x_{k+1} = A_d x_k + B_d u_k$$

where $\mathbf{A}_d$ and $\mathbf{B}_d$ are the discretized state space **A** and **B** matrices and

$$A_d = e^{AT_s}$$

$$B_d = \int_0^{T_s} e^{A\eta}\, d\eta$$

As *Coulomb1.m* steps through for each value of the commanded input, u_c, which is essentialy each time step of 0.01 seconds, the true friction state representation is calculated and discretized. This is, however, after the previous time step estimate of the friction has been added to the input, u, through $u = -k\hat{x}_k$.

3.4.1.2 Coulomb2.m. The second macro that was used to simulate the Coulomb model compensator is identical to *Coulomb1.m* except that is uses a discrete time step of 0.001 seconds instead of 0.01 seconds. This was done to allow the use of very fast estimator poles for comparison purposes. Because of the number of points required to get a reasonable simulation, this version ran very slowly. It was only used when it was suspected that the estimator pole placement exceeded the Nyquist sampling frequency of the simulation.

3.4.2 Dahl Model Compensator Simulation. The Dahl model friction compensator was coded into ProMatlab™ in much the same manner as the Coulomb model compensator was, only using the development described in Section 3.3. The exact code for the Dahl model compensator simulations was called *Extendkf.m* and is given in Appendix B.

The first five lines of the macro set up the initial value of the actual state vector, used for the truth model, and input an initial guess for the estimated state, $\hat{x}$, as well as setting up a counter and initializing the output format. The macro then steps through each time step and value of the commanded input, u_c or Θ_c. The first time through, the macro uses the initial guess of $\hat{x}$ to propogate the true state forward one time step. Subsequent time steps use the $\hat{x}$ that is generated by the extended Kalman filter that was discussed in Section 3.3.

It should be mentioned here that, numerically, the actual Dahl friction value and the estimated friction value may exceed the running friction value, T_c, which we know can't happen. Thus, the macro conducts a check to see if this occurs. If it does occur, the value of the friction torque or estimated friction torque is forcibly set to be equal to the running friction torque, which is essentially the Coulomb model. Physically, this would represent a large deflection of the system, passing through the Dahl friction compliance zone (x_c) which was discussed in Chapter 2. In some sense, then, the Dahl controller is a hybrid controller. When $\Theta_c \approx x_c$, the Dahl friction model prevails and when $\Theta_c >> x_c$, the Coulomb model prevails.

IV. Results

This chapter contains a discussion of the simulations that were conducted with both the Coulomb model and the Dahl model friction compensators. The response characteristics for each compensator and for various input commands were compared, and conclusions were made concerning the advantages/disadvantages of each compensator. These conclusions, along with some recommendations are discussed in Chapter 5. The conclusions that are of particular importance are the ones concerning the Dahl controller results for small deflection inputs. As was mentioned in the intoduction, the focus of the research was investigate if any advantages gained in the use of the Dahl compensator outweigh the added complexity and increase in onboard computing power required for the extended Kalman Filter.

4.1 Simulation Ground Rules and Assumptions

The main assumptions made in the simulation of the friction compensators concerned the system itself (i.e. moment of inertia, Dahl *true* friction parameters, etc.), design specification goals (i.e. overshoot, settling time, max motor torque, etc.), and the commanded input characteristics (Θ_c).

4.1.1 System Assumptions. In order to add credibility to the simulations, a realistic baseline system was used. The specific system parameters such as σ, i, T_c, and J were taken from actual experimental runs

by Dahl (6:60). The following values for the system parameters were used for all of the simulations: σ=5.9 ounces/degree, i=1.44, J=0.6676 inch-ounce/degree/second^2, and T_c=1.78 inch-ounces. The deflection was in degrees. The measurement noise, v, was a randomly generated input with zero mean and an assumed rms magnitude of 10 percent of the smallest commanded input deflections.

4.1.2 Design Specification Goals. For these simulations, time response specifications of overshoot and settling time were arbitrarily set. For a simulation to be considered good, it must meet these specification goals. The maximum allowable overshoot was 10 percent of the overall step input. The maximum settling time was four seconds, where settling time was defined as the time until the response has settled to within $\pm$ two percent of its steady state value. No exact maximum or minimum rates, accelerations, or motor touques were specified. However, these were all taken into account and checked to make sure they were realistic values.

4.1.3 Commanded Input Characteristics. The commanded input used for the Coulomb compensator simulations was a basic step input like the one shown in Figure 4-1. The magnitude of the step varied depending on whether or not the bearing was to be simulated inside of the compliance zone, x_c. To choose the magnitude of the step input, the knee of the Dahl true friction model deflection curve or compliance zone was calculated using the fact that

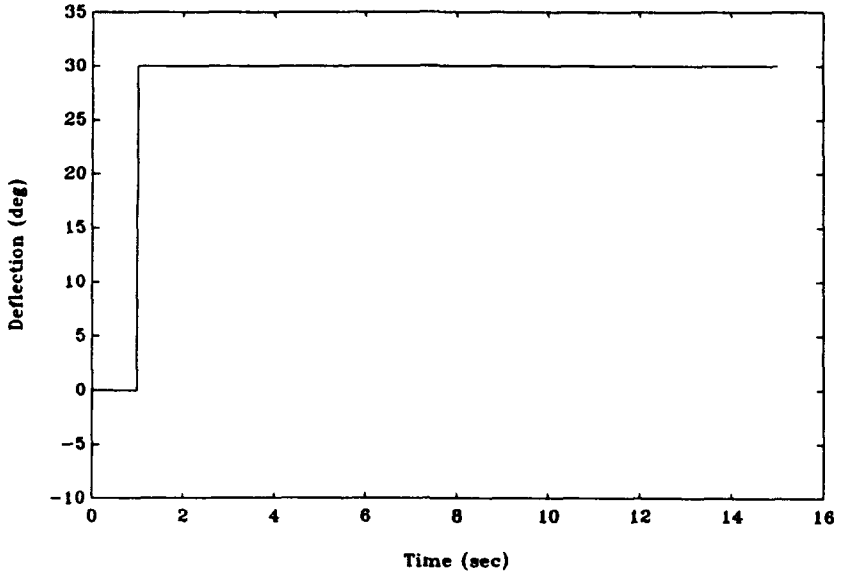

Figure 4-1. Coulomb Controller Step Input

the known rest slope, σ, is just the rise (T_c) over the run (x_c), or

$$x_c = \frac{T_c}{\sigma}$$

For this system with the assumed parameters $x_c \approx 0.3$ degrees. Thus, the commanded step inputs for simulations inside the compliance zone are on the order of 0.25 degrees, while those for simulations outside the compliance zone are on the order of 30 degrees.

The commanded inputs used in the Dahl model compensator were slightly more complex than those used for the Coulomb compensator. A

combination square wave and step input similar to that shown in Figure 4-2 was used. The reason for this was to cycle the extended Kalman filter through a period or two of a square wave to allow the estimations of the Dahl friction parameters to converge. Following the square wave the system was hit with a constant step as in the Coulomb simulations. Since the system parameters

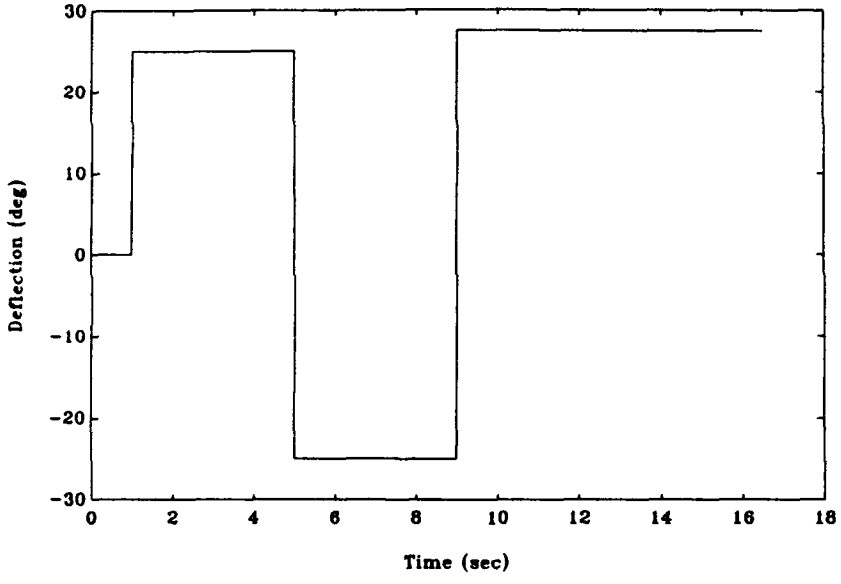

Figur 4-2. Dahl Controller Input

were the same for both compensators, the compliance zone is also the same, $x_c \approx 0.3$ degrees. Thus, the magnitude of the Dahl compensator simulation inputs were similar to those for the Coulomb compensator simulations.

Since most of the simulations were run with a relatively large time step of 0.01 seconds to minimize simulation time, the smallest magnitude of the commanded inputs for the small deflection simulations was 0.25 degrees. In

using deflections much smaller than that, the simulation could be susceptible to errors caused by the numerical integration with the relatively large time step.

4.2 Simulation Results

This section describes the specific procedures and results of each simulation made using both the Coulomb compensator and the Dahl compensator.

4.2.1 Coulomb Model Compensator Results. The basic procedure used to simulate the Coulomb friction compensator was as follows. Regulator and estimator gains, **k** and **L**, were found using the *Place* command in ProMatlab™ as mentioned in chapter 3. The regulator and estimator poles were arbitrarily placed, keeping in mind that the frequency of the regulator/estimator poles should be less than one tenth (0.10) of the frequency of numerical integration time step. Using this initial pole placement, the macro was run and the deflection time response was plotted to see if the specification goals were met. If not, the estimator and/or regulator poles were moved to change their frequency and damping characteristics, and new gains, **k** and **L** were generated. The macro was run again and the deflection time response checked. This procedure was repeated until acceptable time responses were achieved. Other parameters besides time responses of the deflections were also checked. Convergence of the estimate to the actual state

and rate response was examined. This was done for both large and small magnitude commanded input deflections. It was also done for simulations with and without noise.

Once good values of **k** and **L** were found for both large and small deflection inputs, these gain values were run on the other input. For example, if $\mathbf{k}_{small}$ and $\mathbf{L}_{small}$ were the regulator and estimator gains that worked for the small deflection, they were then used to run a simulation with a large deflection and vice versa. This was done to assess the *robustness* of the system. If the controller did not perform well for both the large deflection and the small deflection inputs using the same gains, it can probably be assumed that some sort of gain scheduling must be employed. This is a factor to consider when comparing comensator designs.

4.2.1.1 Coulomb Large Deflection Results. The first Coulomb compensator runs were made without noise. Since the integration time step for *Coulomb1.m* was 0.01 seconds, which has a frequency of 200π rads/sec, the estimator poles can be chosen with a frequency as high as 20π rads/sec. As an initial starting point, the estimator poles were chosen at s=-10, -10, and -10. The regulator poles were initially chosen to be $s=-0.5\pm0.5j$. This produced the following set of gains: **k**=[0.3338 0.6676 -1] and **L**=[30 300 -667.58]^T. The time response of the position for these gain values is shown in Figure 4-3.

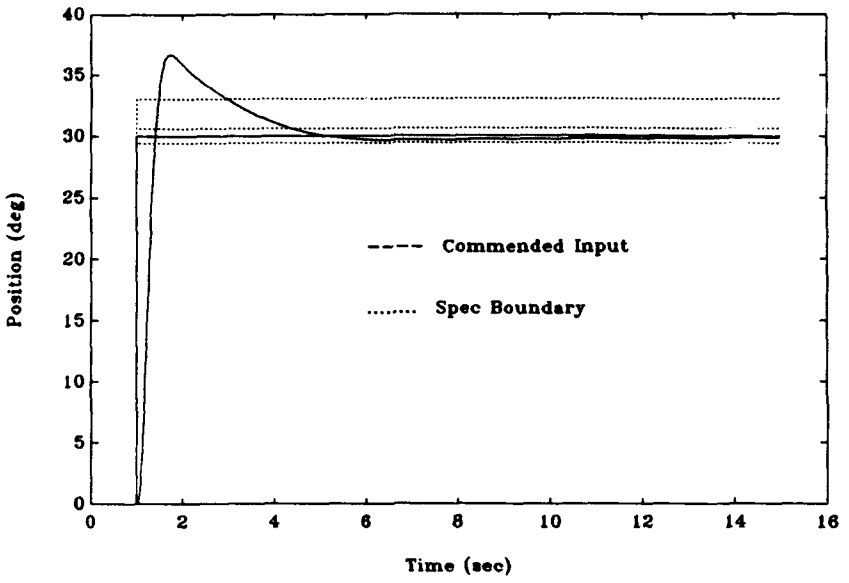

Figure 4-3 Coulomb Large Input Initial Try

After a few iterations, the estimator poles were placed at s=-60$\pm$2j and (s+60) and the regulator poles were placed at s=-0.5$\pm$1.5j)] yielding gains of **k**=[1.6690 0.6676 -1] and **L**=[180 10,804 -144,375.5]^T. The resulting deflection time response is shown in Figure 4-4. This still did not meet the spec requirement for overshoot. In order to meet this requirement, the estimator poles had to be put at way out a (s+75), (s+75), and (s+75), which is beyond the bandwidth of the contoller. Thus, the other simulation macro, *Coulomb2.m* had to be used. The regulator poles for this simulation were placed at [s+(.75+1.75j)] and[s+(.75-1.75j)]. Figure 4-5 shows the Θ

response using these very high estimator poles. The estimates of position, rate, and friction torque were plotted with the actual state to check for convergence of the estimate. These are plotted in Figures 4-5a, 4-5b, and 4-5c. It would appear that the estimate converges very nicely except for the position. This is because the commanded input, Θ_c was added in the Luenberger estimator in Chapter 3. This has also been demonstated by Liebst (9).

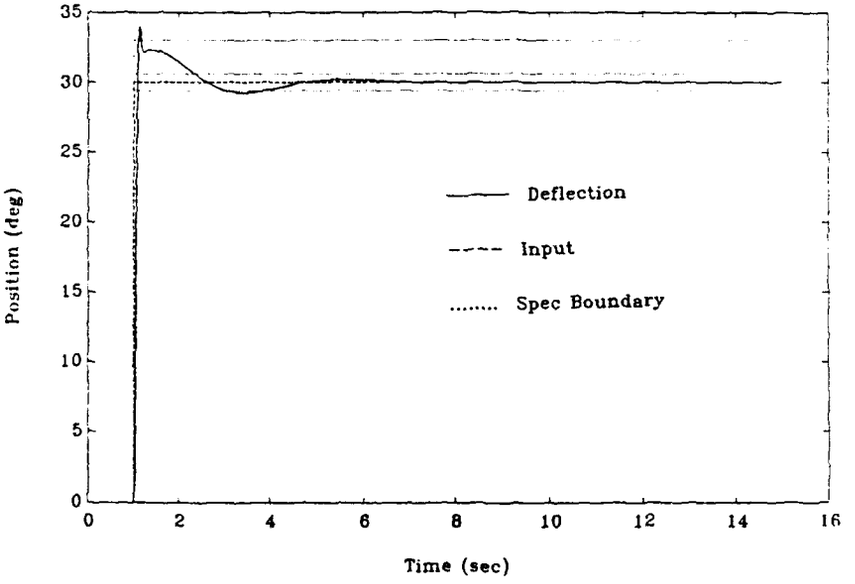

Figure 4-4 Coulomb1.m with Large Input -- Pushing the Bandwidth of the Controller

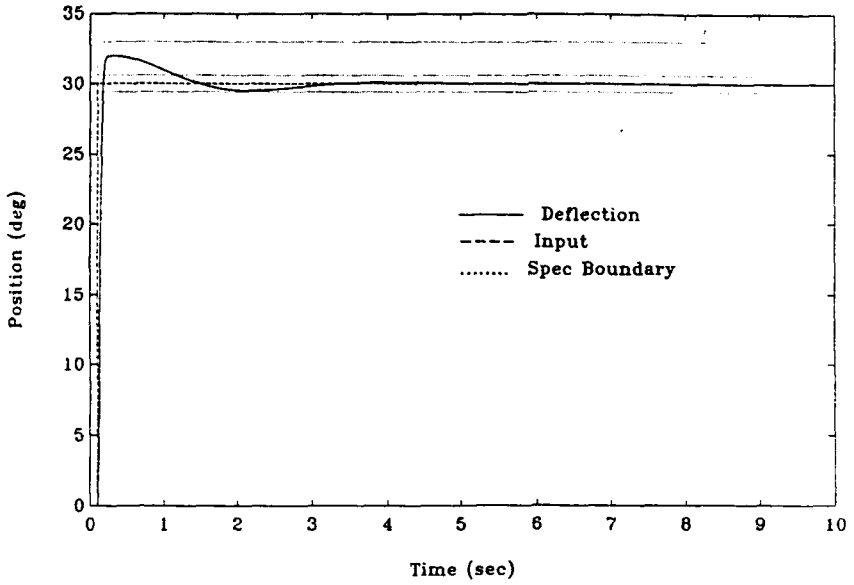

Figure 4-5 Simulation with Very Fast Estimator Poles Run Using Coulomb2.m

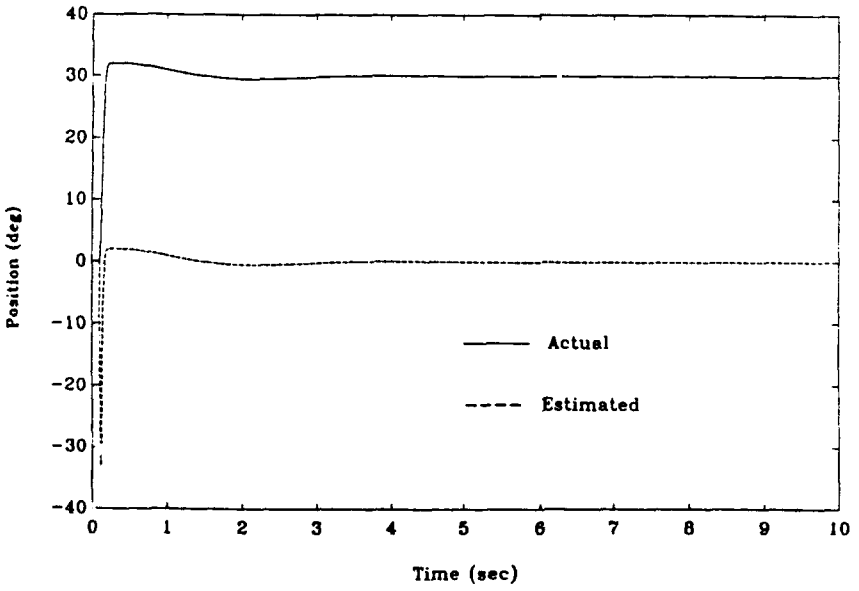

Figure 4-5a Actual and Estimated Position

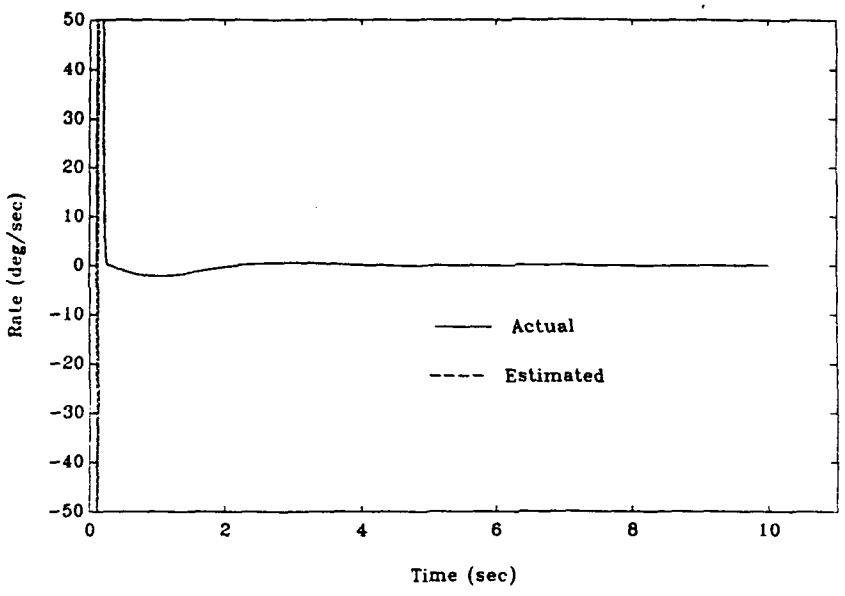

Figure 4-5b Actual and Estimated Rate

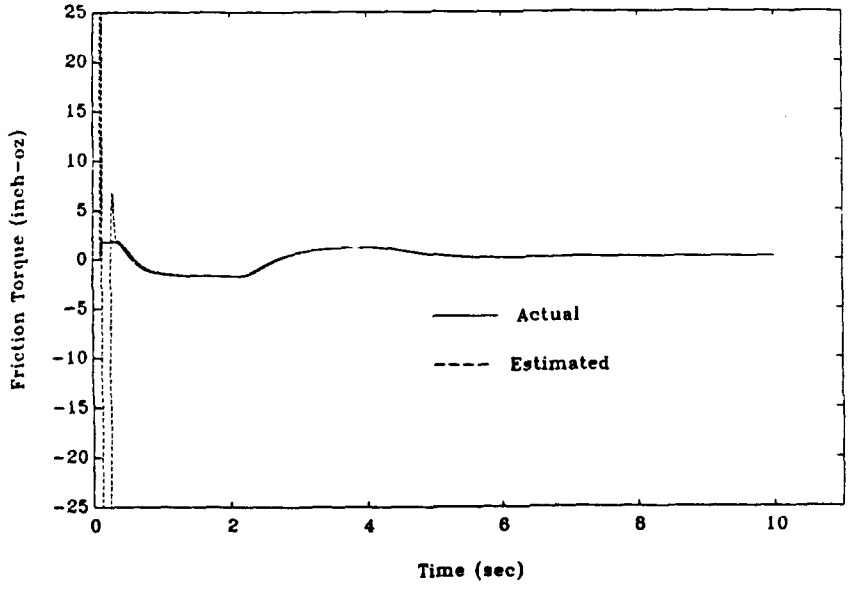

Figure 4-5c Actual and Estimated T_F

4.2.1.2 Coulomb Small Deflection Results. The same basic procedure that was used with the large deflection simulations was also used with the small deflection simulations. For brevity, the initial pole placement trials will not be discussed. Figure 4-6 shows the position time response for a small deflection with the estimator poles at $s=-12\pm2j$ and $s=-12$ and the regulator poles at $s=-0.5\pm,1.5j$, which yields gains of $\mathbf{k}=[1.6690\ 0.6676\ -1]$ and $\mathbf{L}=[360\ 436\ -1185.6]^T$. Here again, the estimate of the state was checked for convergence in Figures 4-6a, 4-6b, and 4-6c.

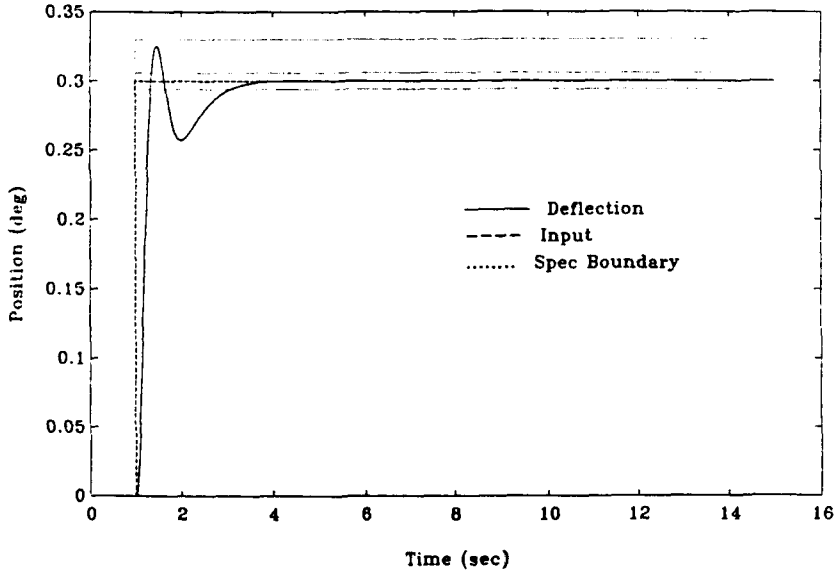

Figure 4-6 Coulomb Small Deflection Input

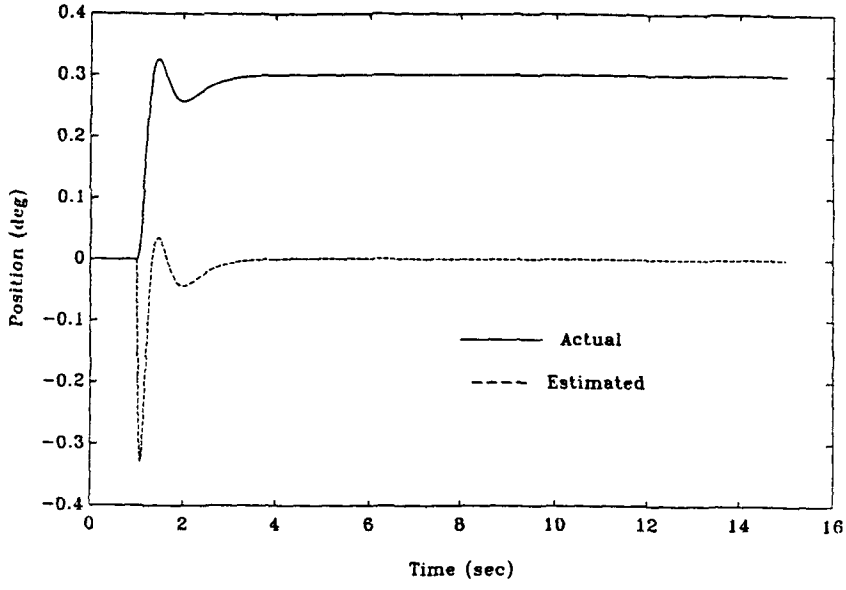

Figure 4-6a Actual and Estimated Position

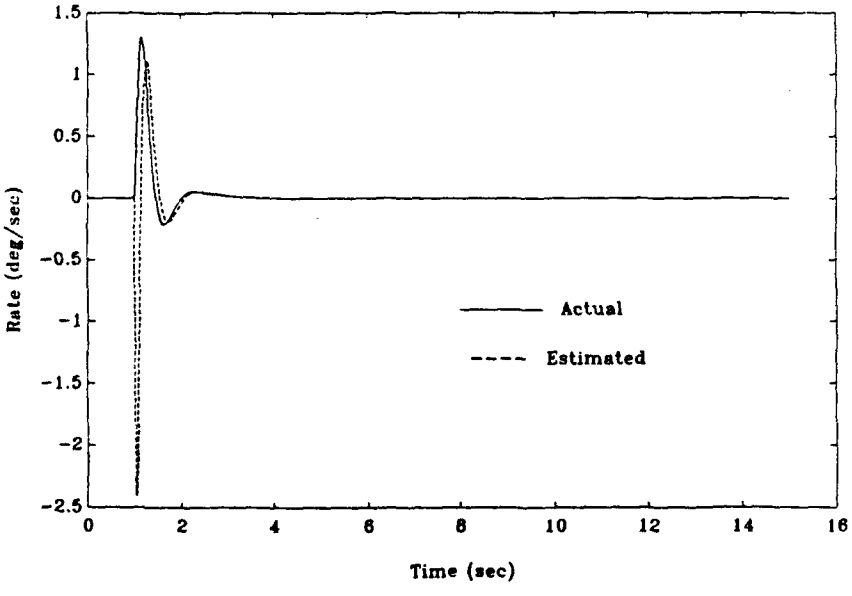

Figure4-6b Actual and Estimated Rate

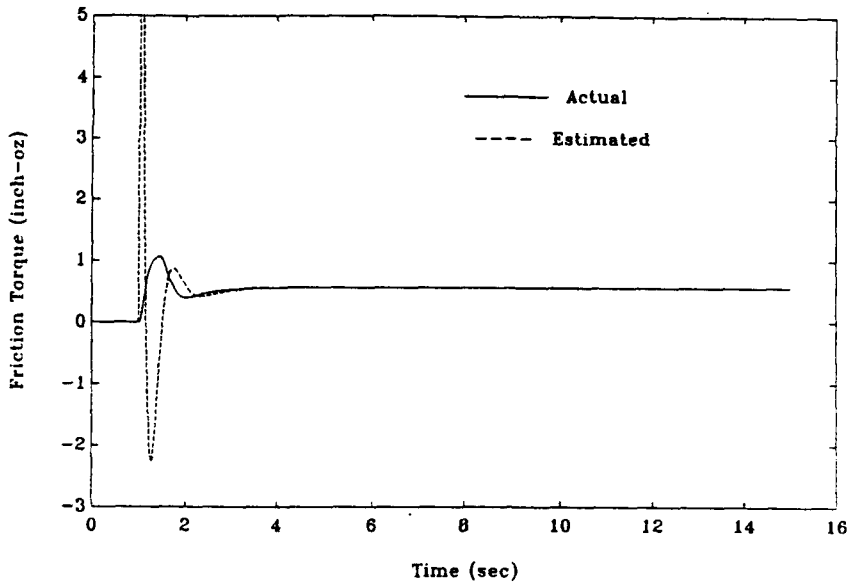

Figure 4-6c Actual and Estimated T_F

4.2.1.3 Coulomb Results with Noise. The previous compensators were run again, only this time a randomly generated, zero-mean noise with a rms magnitude of 10 percent of the small step input was added to the measurement. The position time responses are shown in Figures 4-7 and 4-8 for both the large and small step inputs. Clearly, since the noise is relatively large compared to the small deflection input, it has a greater effect on the time response. Still, the mean response follows the same general shape as the ones without the measurement noise. Figures 4-7a through 4-7c and 4-8a through 4-8c show the actual and estimated states for both of these simulations with noise.

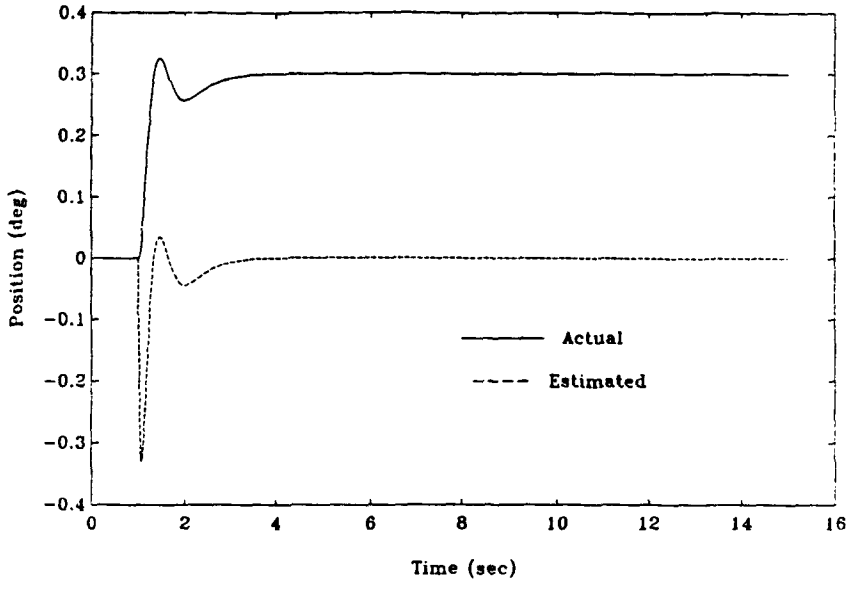

Figure 4-6a Actual and Estimated Position

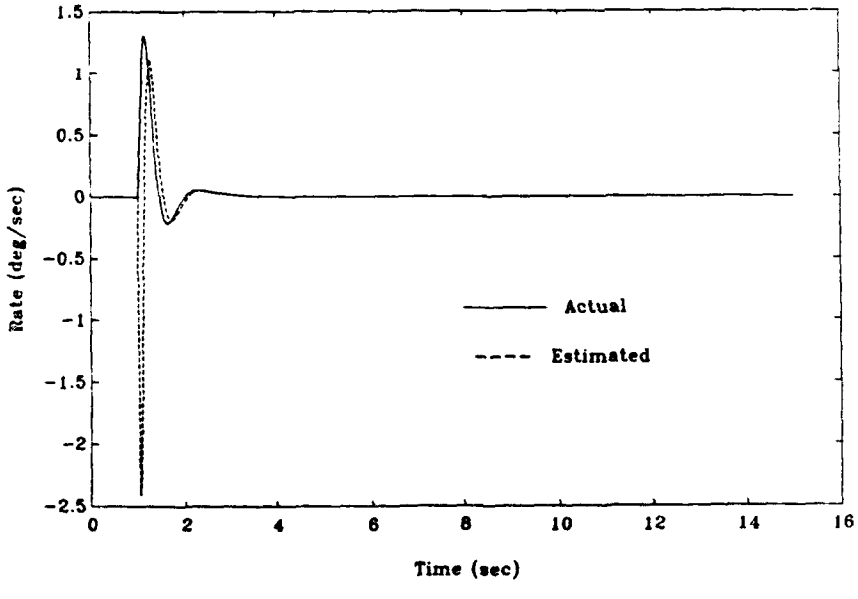

Figure4-6b Actual and Estimated Rate

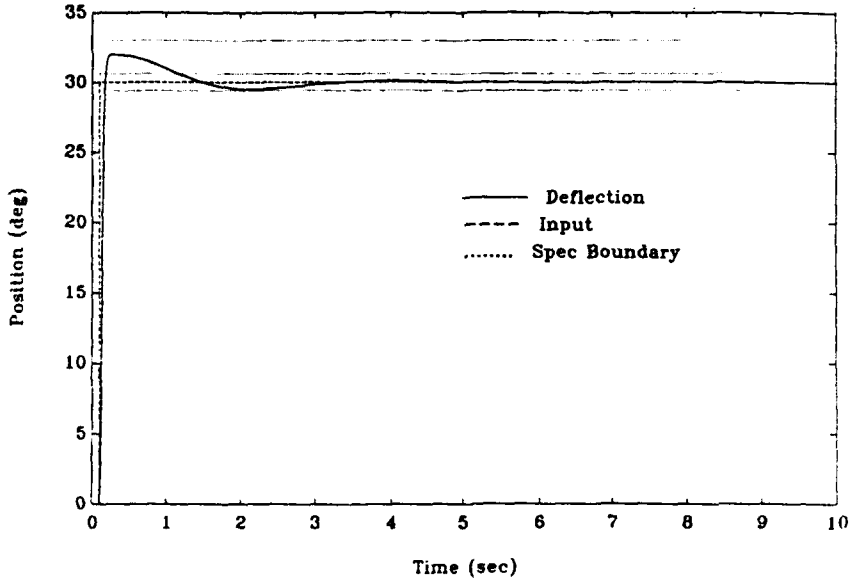

Figure 4-7 Coulomb Large Input with Noise

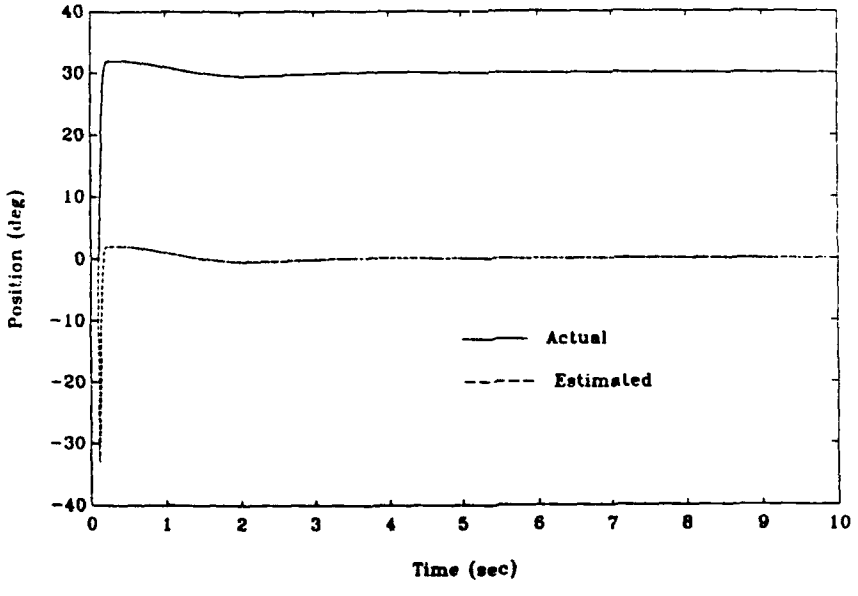

Figure 4-7a Actual and Estimated Position

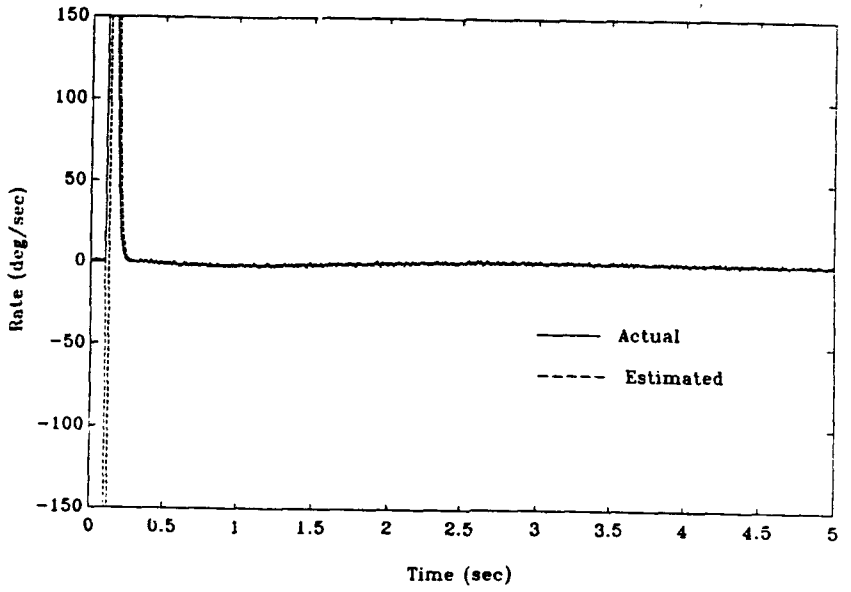

Figure 4-7b Actual and Estimated Rate

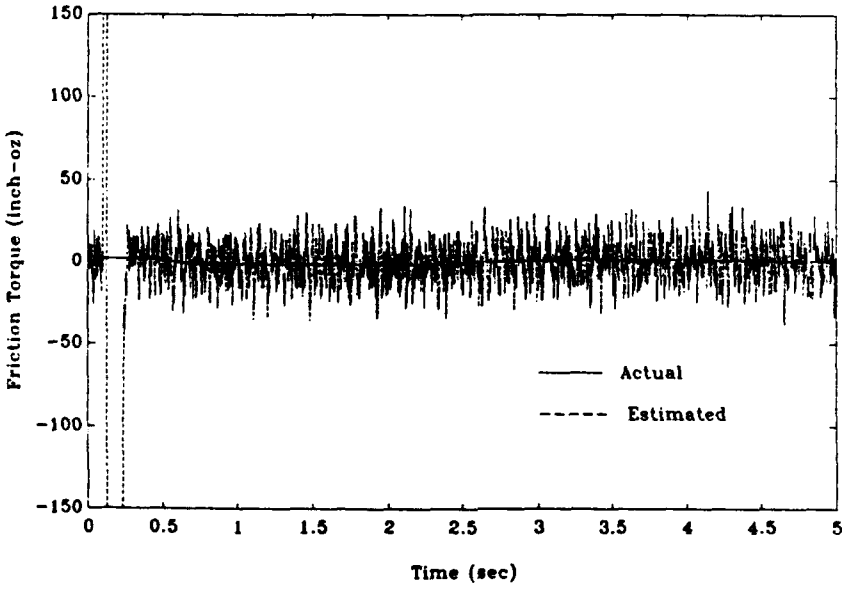

Figure 4-7c Actual and Estimated T_F

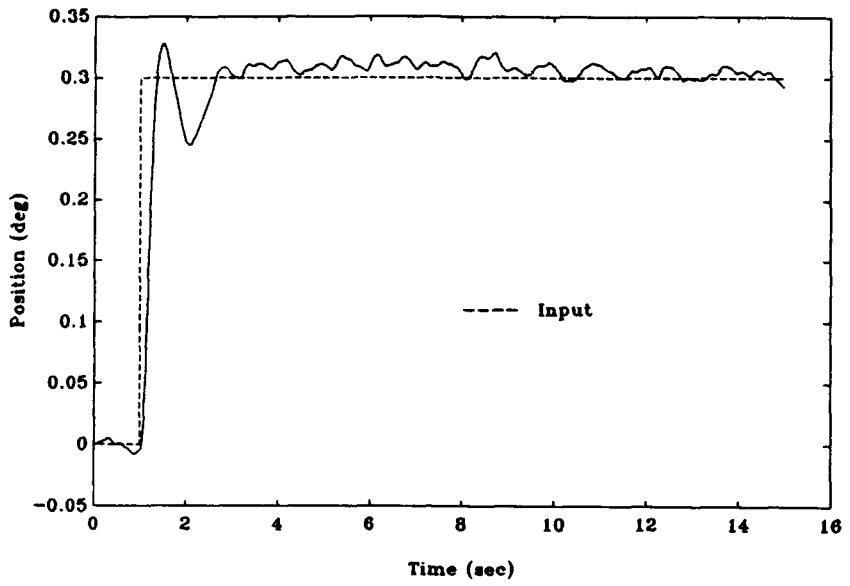

Figure 4-8 Coulomb Small Input with Noise

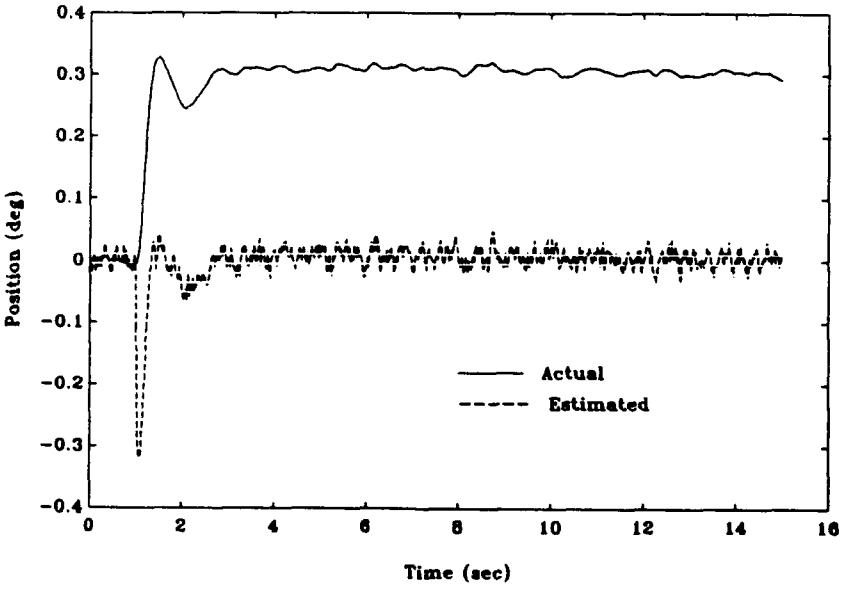

Figure 4-8a Actual and Estimated Position

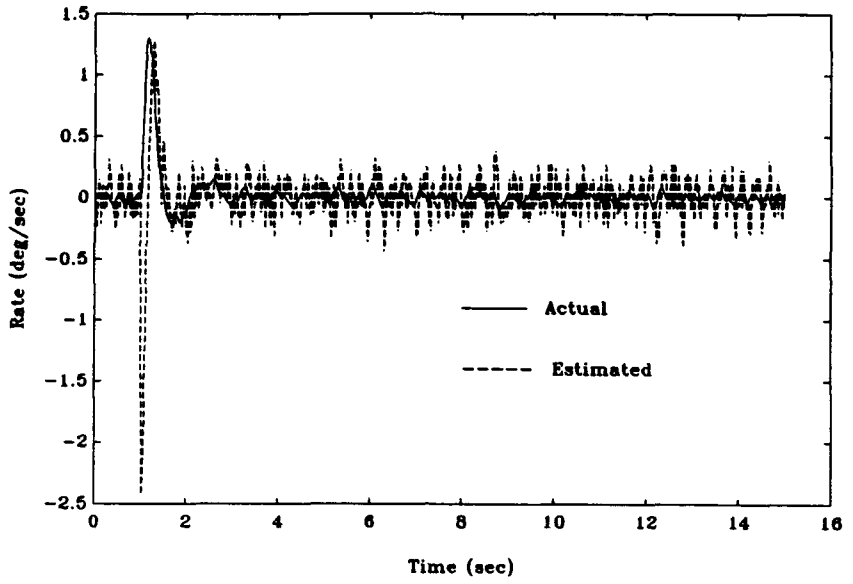

Figure 4-8b Actual and Estimated Rate

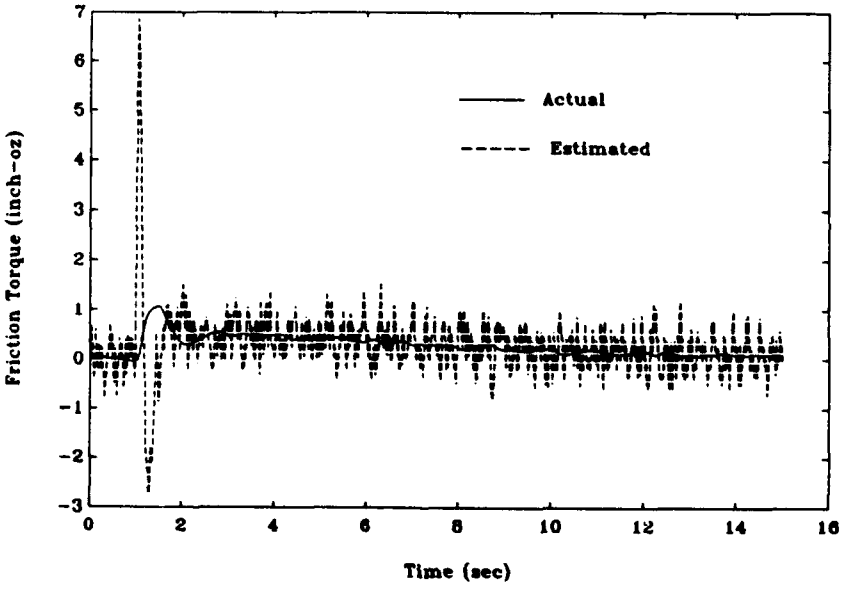

Figure 4-8c Actual and Estimated T_F

4.2.1.4 Coulomb Simulation Robustness Check. As a form of *robustness* check, regulator and estimator gain values were run with the other commanded input. This was done to see if the compensator could handle large variations in gains and still meet performance requirements. Figure 4-9 shows the position time response for small deflection gains run with a large deflection input. Figure 4-10 showa the position time response of the large gains run with a small deflection input.

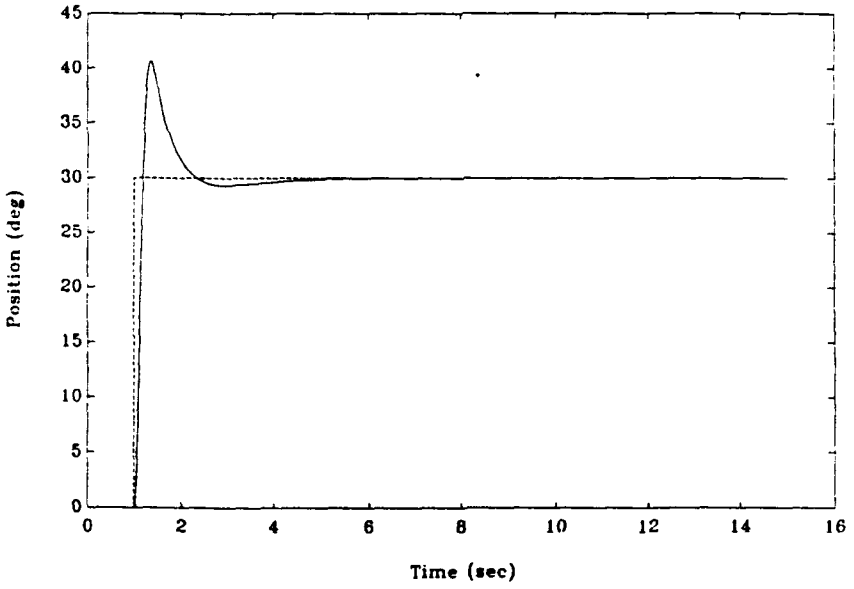

Figure 4-9 Position Response for Large Deflection Input Using Small Deflection Gains

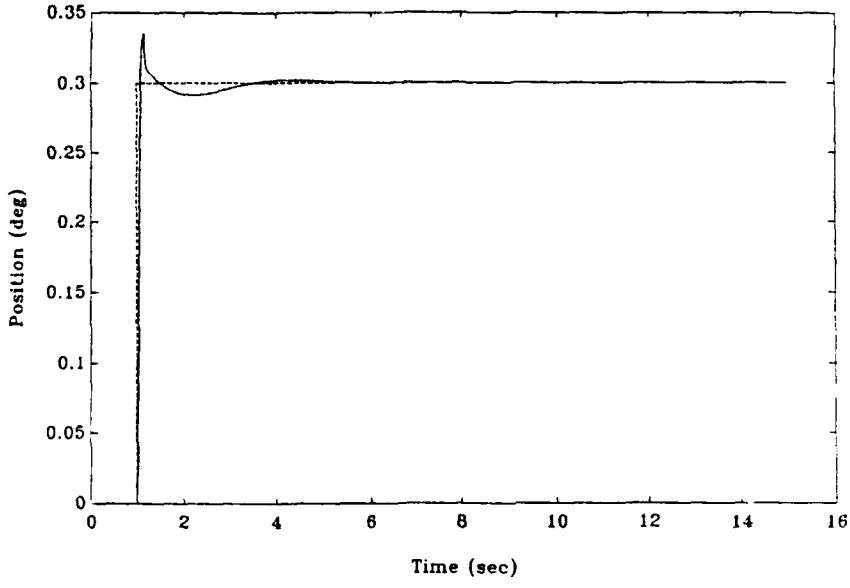

Figure 4-10 Position Response for Small Deflection Input Using Large Deflection Gains

4.2.2 Dahl Model Compensator Results. The Dahl model friction compensator simulations were run in a manner similar to the Coulomb simulations. One major difference was that the Dahl compensator did not need to be given estimator gains, **L**. These were calculated internally in the extended Kalman filter, and are time varying. Thus, only the regulator poles were placed and regulator gains calculated for this compensator.

There was also, however, the very difficult task of determining all of the weights that the extended Kalman filter uses in its estimation propagation. These include R, Q, and G and were discussed in Chapter 3. To find these weights, numerous simulations of the extended Kalman filter were made in

both open and closed loop configurations. By individually changing the weights and observing the effect each has on the system, ranges of the weight values were determined. The system was very sensitive to these weight values. This sensitivity will be discussed throughout the remainder of this thesis in more detail.

4.2.2.1 Dahl Large Deflection Results. The Dahl compensator simulations were also run without noise at first. The procedure was very similar to that of the Coulomb simulations. An initial run was made and the position time response was looked at. Changes were made to the regulator pole placement to change the regulator gains, **k**, along with changes to the weights **Q**, and **R**, to get the desired response characteristics. Figure 4-11 shows the position time response to a large deflection commanded input with the regulator poles placed at $s=-3\pm0.5j$ which produces a gain of **k**=[6.1751 4.0055 -1]. The weights used in this particular run were

$$\boldsymbol{Q} = \begin{bmatrix} 0 & 0 & 0 & 0 & 0 \\ 0 & 10 & 0 & 0 & 0 \\ 0 & 0 & 0 & 0 & 0 \\ 0 & 0 & 0 & 30 & 0 \\ 0 & 0 & 0 & 0 & 40 \end{bmatrix} \quad ; \quad \boldsymbol{R} = 1 \quad ; \quad \boldsymbol{G} = \boldsymbol{I}$$

Plots of the actual and estimated state were made to check for convergence, just as with the Coulomb simulations. These are shown in Figures 4-11a through 4-11c. It would appear from these plots that the extended Kalman

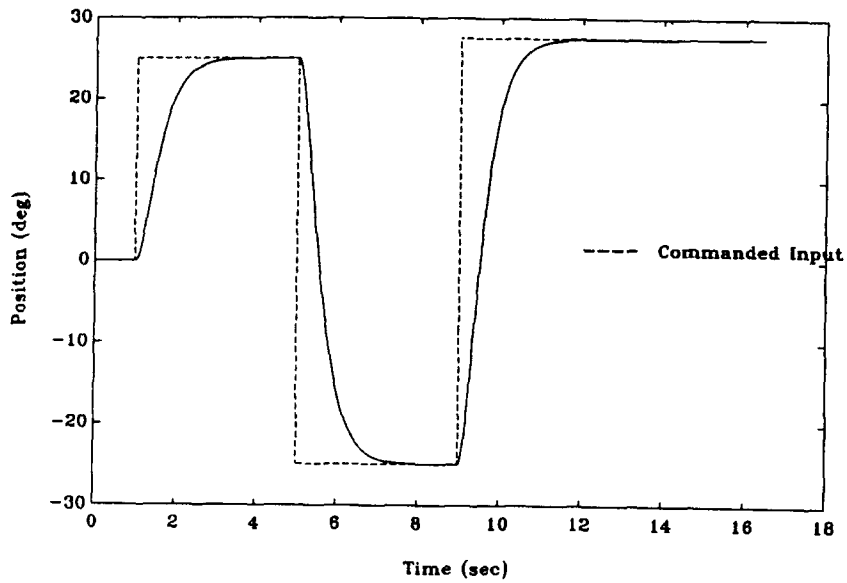

Figure 4-11 Dahl Large Deflection Input

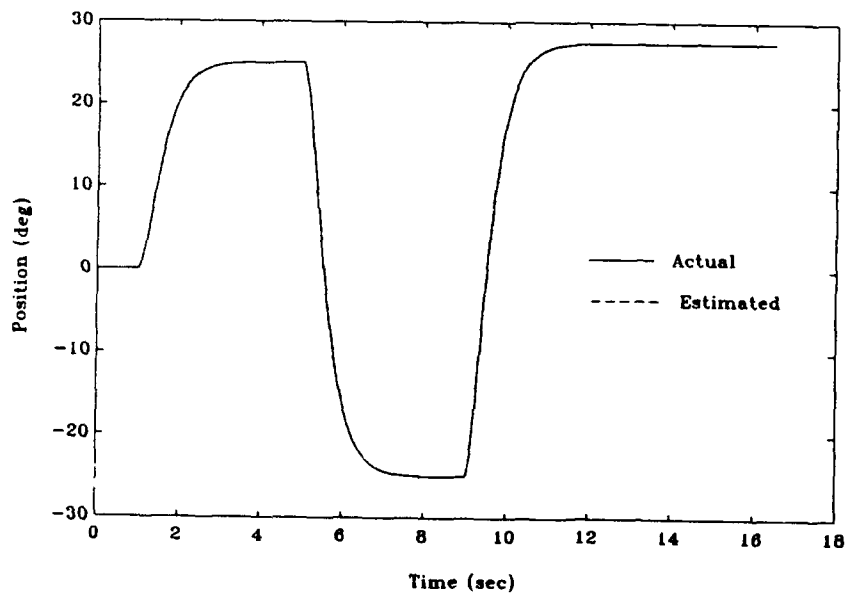

Figure 4-11a Actual and Estimated Position

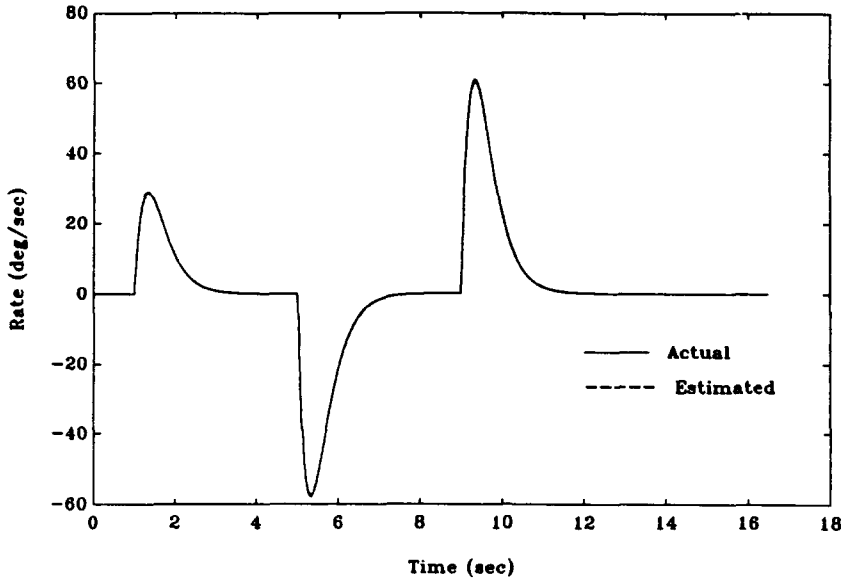

Figure 4-11b Actual and Estimated Rate

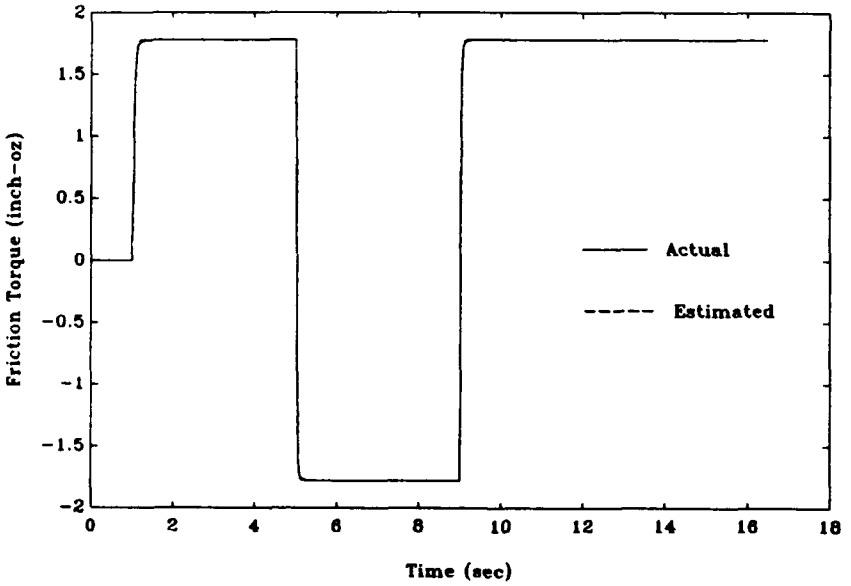

Figure 4-11c Actual and Estimated T_F

filter is doing an excellent job of estimating the states. This is due to the fact that the system is not in the compliance zone for very long. Thus, the system is spending most of the time at the running friction value, which is known, and the estimator does not have to work very hard to get a good estimation. Subsequent runs for the large deflection inputs were made with commanded inputs that excited the system with a series of small square waves that were within the compliance zone. The time responses for these simulations were very similar to those shown previously. Unlike the Coulomb controller, the Dahl compensator does not experience the quasi-estimation of the position state, Θ, due to the incorporation of the commanded input, Θ_c.

4.2.2.2 Dahl Small Deflection Results. The same procedure that was used for the large deflection input was also used for the small deflection input. The final values chosen for the weights were

$$\boldsymbol{Q} = \begin{bmatrix} 0 & 0 & 0 & 0 & 0 \\ 0 & .01 & 0 & 0 & 0 \\ 0 & 0 & 0 & 0 & 0 \\ 0 & 0 & 0 & 25 & 0 \\ 0 & 0 & 0 & 0 & 30 \end{bmatrix} \quad ; \quad \boldsymbol{R} = 1 \quad ; \quad \boldsymbol{G} = \boldsymbol{I}$$

The regulator poles were placed in the same location as before so that $\mathbf{k}=[6.1751\ 4.0055\ -1]$. The time response of Θ is shown in Figure 4-12. The actual and estimated state variables are plotted in Figures 4-12a through 4-12c. Here again, the estimate converges very quickly to the actual values.

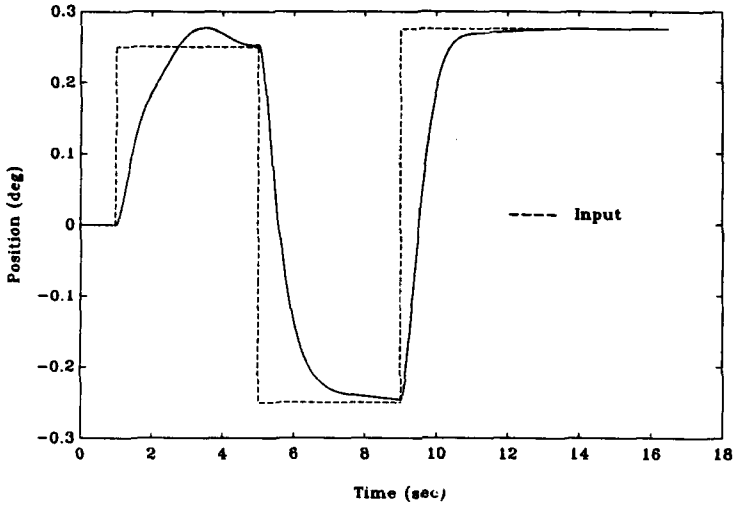

Figure 4-12 Dahl Small Defection Input

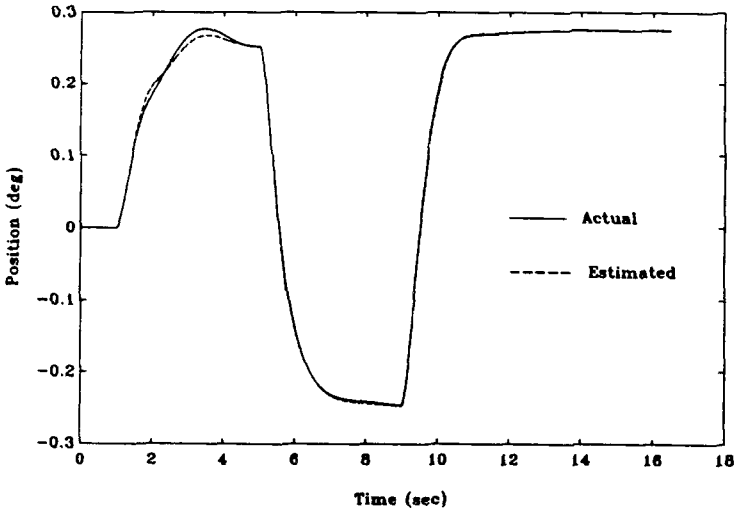

Figure 4-12a Actual and Estimated Position

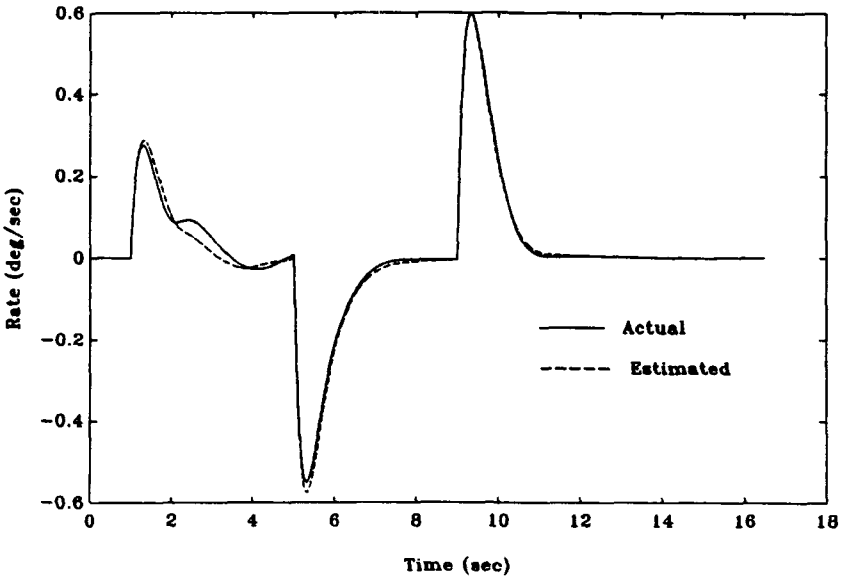

Figure 4-12b Actual and Estimated Rate

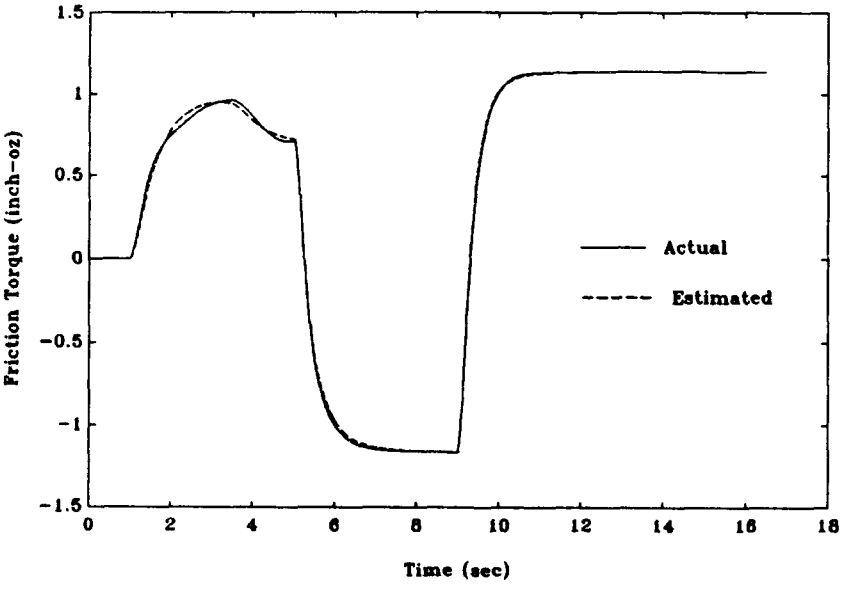

Figure 4-12c Actual and Estimated T_F

4.2.2.3 Dahl Results with Noise. Both Dahl compensators from the last two sections were run with a measurement noise. The noise, v, was identical to that used in the Coulomb simulations. The position response for the large input is plotted in Figure 4-13 and for the small input in Figure 4-14. Contrasting to the Coulomb noise simulations, the Dahl compensator does not seem to be effected by noise very much at all. The estimates of position, rate, and friction torque are plotted with the actual values in Figures 4-13a through 4-13c for the large deflection and in Figures 4-14a through 4-14c for the small deflection. Here we can see that the noise does not seem to effect the estimation convergence as much as it did in the Coulomb simulations, especially in the estimation of friction torque, T_F. For the most part this is true; however, from Figure 4-13c it is possible that the estimate of T_F is not converging to the actual value. Upon inspection of σ and i, it was found that the estimate of σ and i were not converging smoothly towards the actual values. It is suspected that this is caused by the sensitive nature of the weights **Q** and **R**. Since the system was not acting within the compliance zone for most of the simulation, additional runs were made where the system was cycled through a series of square waves within the compliance region to allow the Dahl parameters to converge before hitting it with the large deflection step. The position and friction torque responses for this simulation are shown in Figures 4-13d and 4-13e.

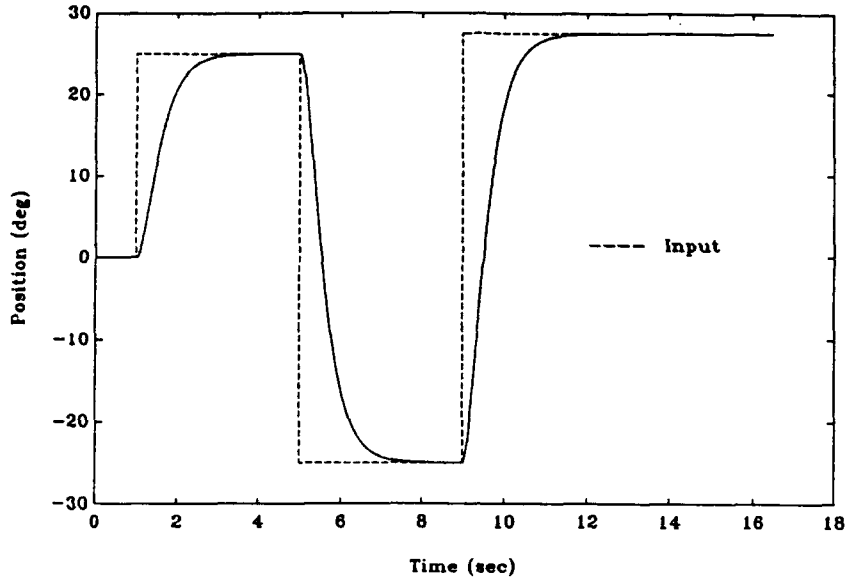

Figure 4-13 Dahl Large Deflection with Noise

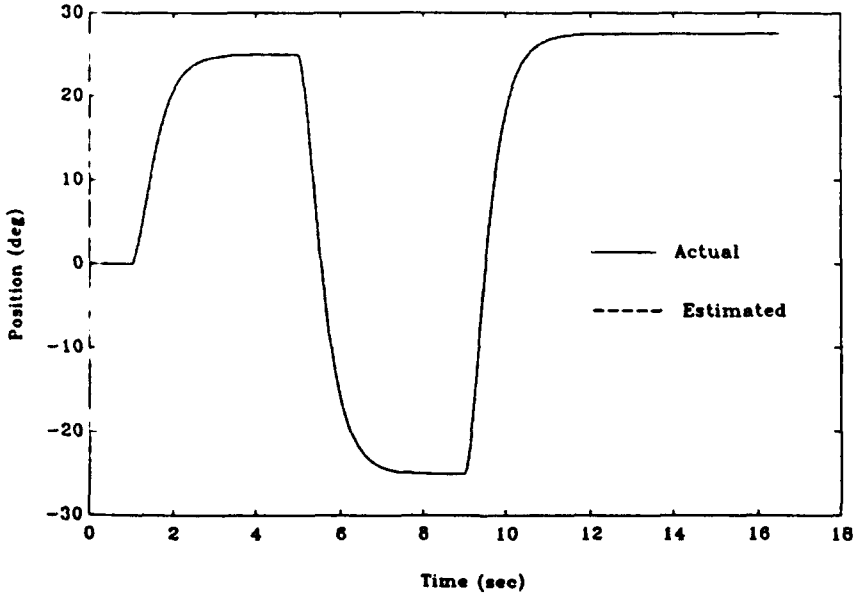

Figure 4-13a Actual and Estimated Position

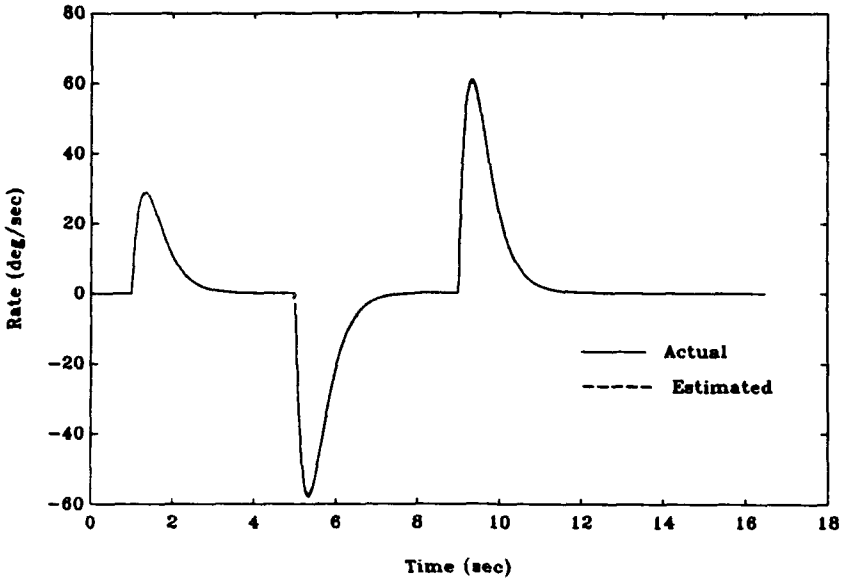

Figure 4-13b Actual and Estimated Rate

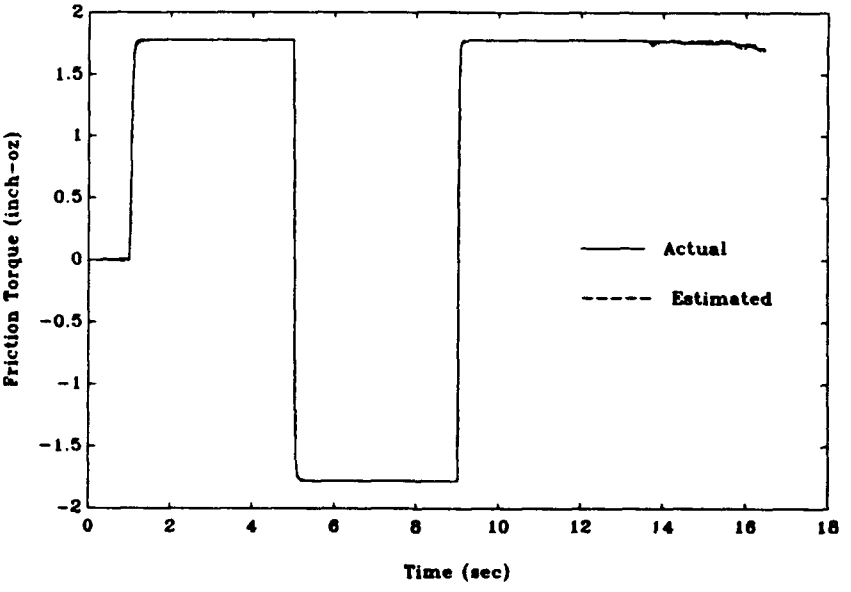

Figure 4-13c Actual and Estimated T_F

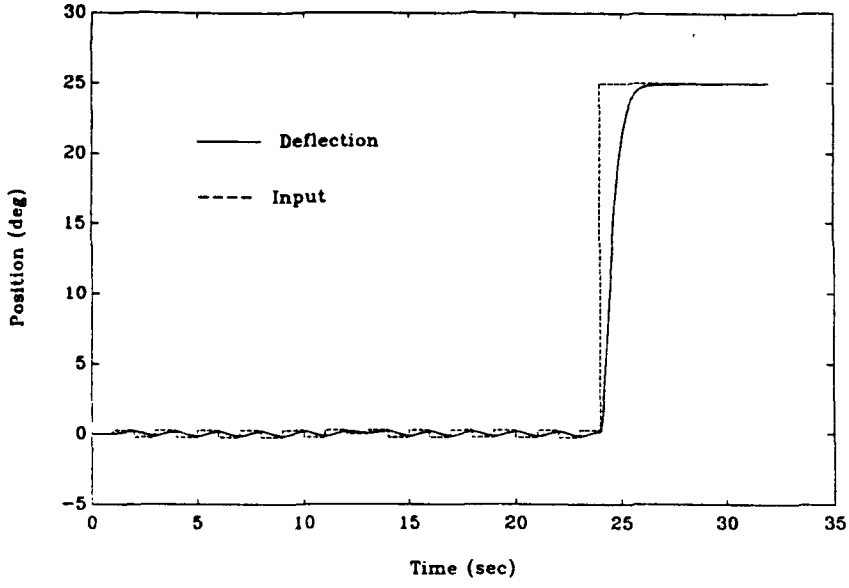

Figure 4-13d Excitation Prior to Large Deflection Input

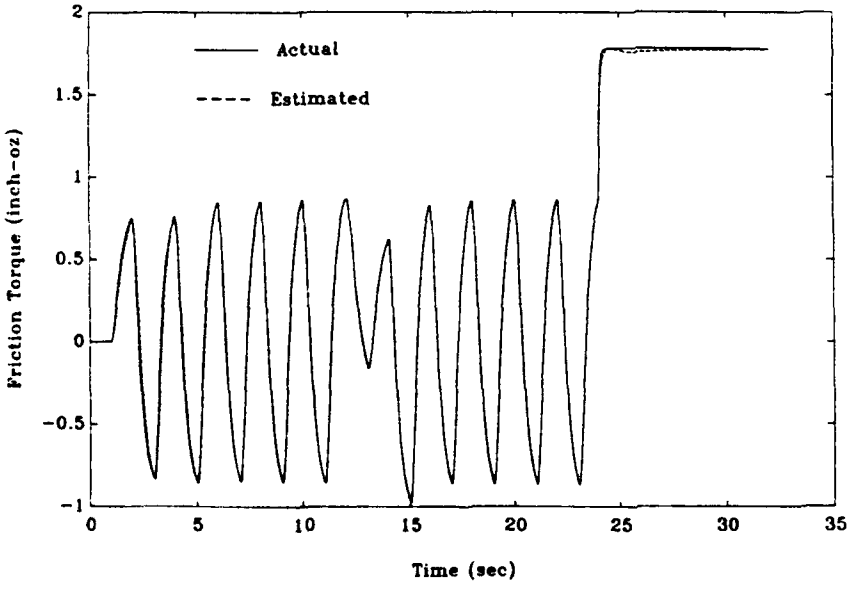

Figure 4-13e Actual and Esimated Friction Torque for Excitation of System Prior to Input

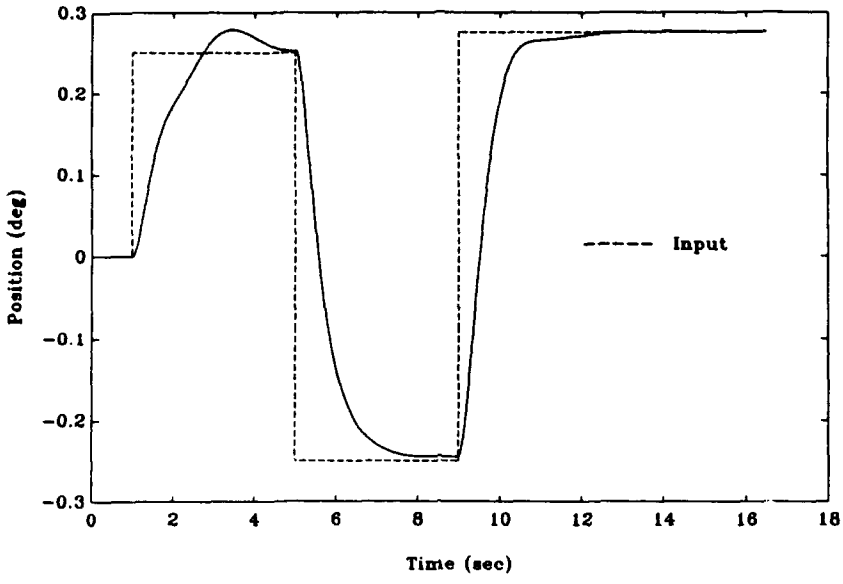

Figure 4-14 Dahl Small Defection with Noise

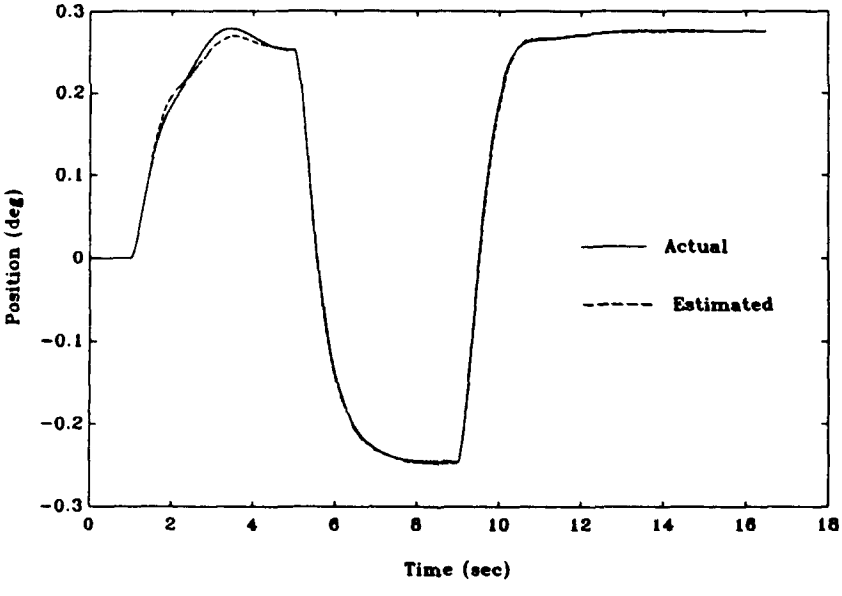

Figure 4-14a Actual and Estimated Position

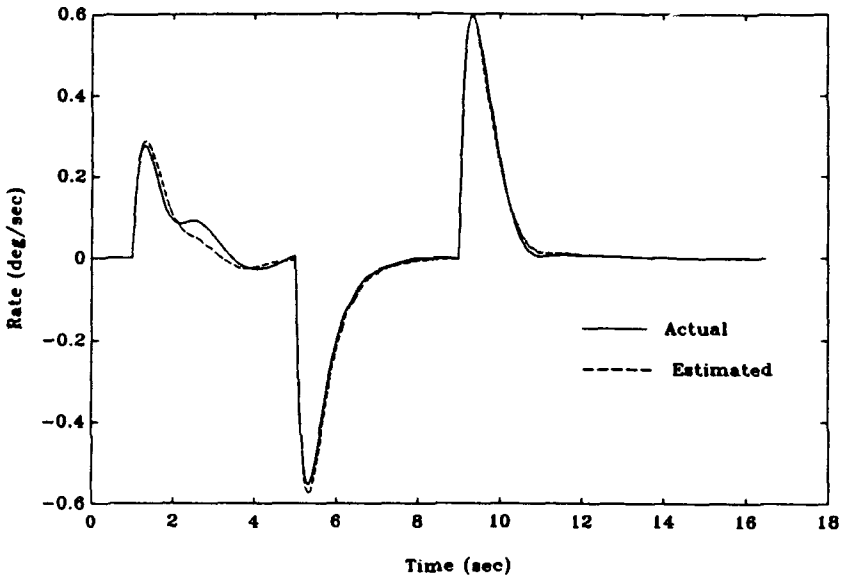

Figure 4-14b Actual and Estimated Rate

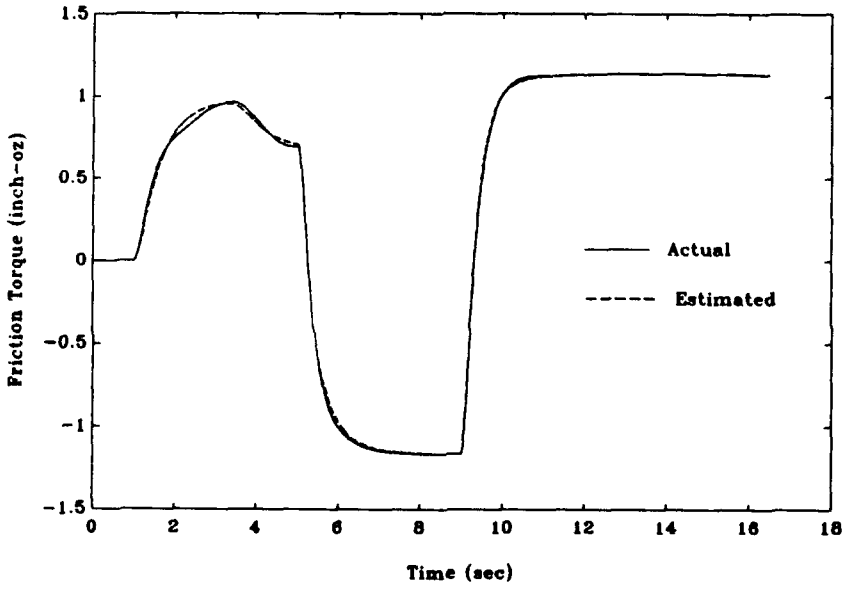

Figure 4-14c Actual and Estimated T_F

4.2.2.4 Dahl Simulation Robustness Check. Like the Coulomb compensator, a *robustness* check was conducted on the Dahl model compensator. As with the Coulomb controller, the gain and weight values developed for the large deflection inputs were run with a small deflection input and vice versa. Figure 4-15 shows the position time response for a small deflection input using the regulator gains and weights used for the large deflection simulation earlier. Clearly, the Θ response is within the

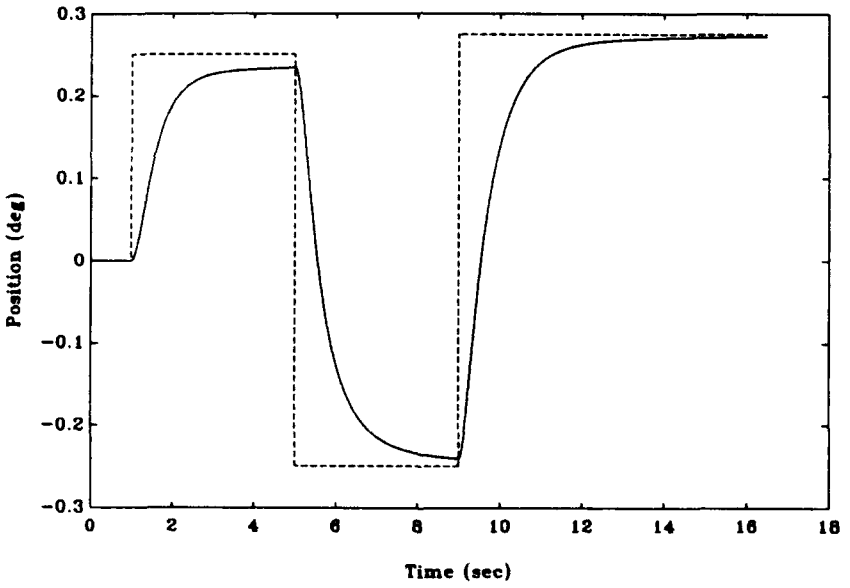

Figure 4-15 Position Response for Small Deflection Input Using Large Deflection Gains snd Weights

specification limits. Figures 4-15a through 4-15c also show that the estimate seems to be converging to the actual values. For this system, regulator gains, weightings, and set of input deflections, the Dahl controller is *robust* enough to handle both commanded input deflections.

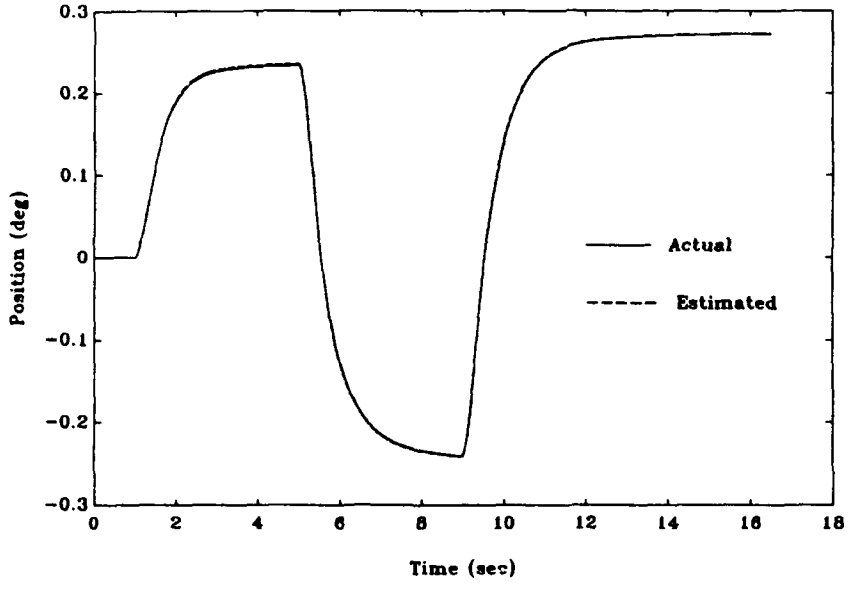

Figure 4-15a Actual and Estimated Position

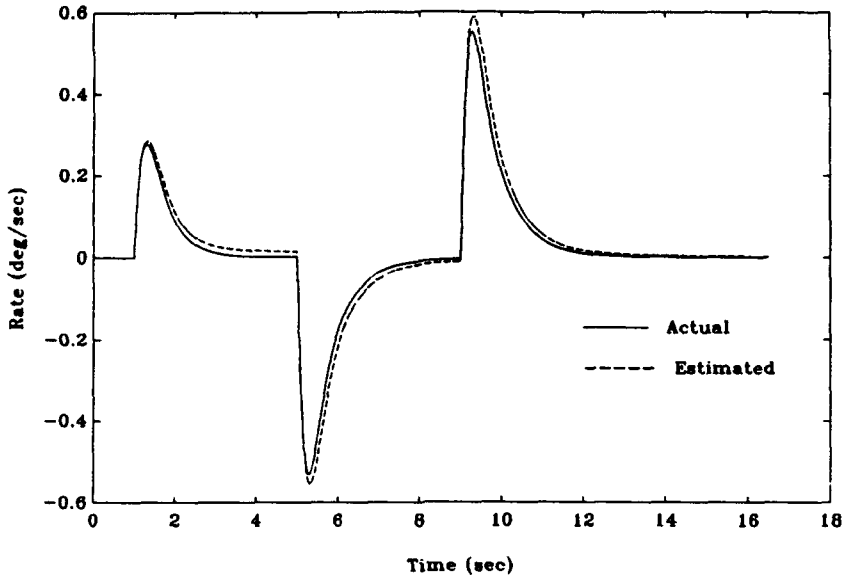

Figure 4-15b Actual and Estimated Rate

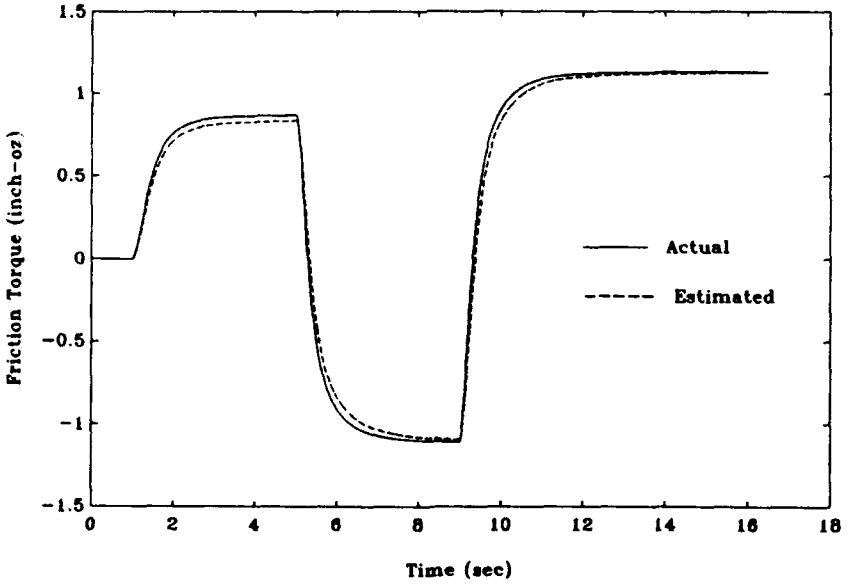

Figure 4-15c Actual and Estimated T_F

However, in the opposite case, where the small deflection gains and weights were run with the large deflection input, the simulation diverged. The weights were such that the estimation of σ and i were divergent, causing the estimate to blow up. This is another example of the sensitivity of the weights **Q** and **R**, since, in other simulations, identical weights did run fine with both large and small deflection inputs, but the performance requirements were not met quite as well or noise rejection characteristics were not as good.

V. Conclusions and Recommendations

5.1 Conclusions

Using the data presented in Section 4.2, along with observations made from the numerous simulations not shown in this thesis, some conclusions can be drawn as to how these two compensators compare to each other. Some of the factors that were looked at in this comparison were: performance in meeting the specification goals, measurement noise rejection properties, computing power required, maximum motor torques, maximum gimbal rates, and robustness to the size of input commands.

5.1.1 Motor Torques and Gimbal Rates. It was shown in section 4.2 that both compensator designs were able to meet required performance specifications for both input deflections. In some sense, the Dahl controller exhibited much smoother response chacteristics than the Coulomb compensator. There was little, if any, overshoot with the Dahl compensator and very reasonable rise times were achieved. In fact, the rise times could have been reduced even further by making the regulator poles faster, at the cost of increasing the control input. The Coulomb controller had very good rise times due to the very high frequency estimator poles. This, however, led to considerable overshoot problems.

The high frequency estimator poles in the Coulomb compensator also caused other problems in terms of the max torques and max rates. Figure 5-1 shows the motor torque (T_m) for a large input deflection simulation using the Dahl controller. The max motor torque required in this simulation was around 300 inch-oz. Figure 5-2 shows the motor torque for the Coulomb compensator for the large deflection input. Here the max required T_m is

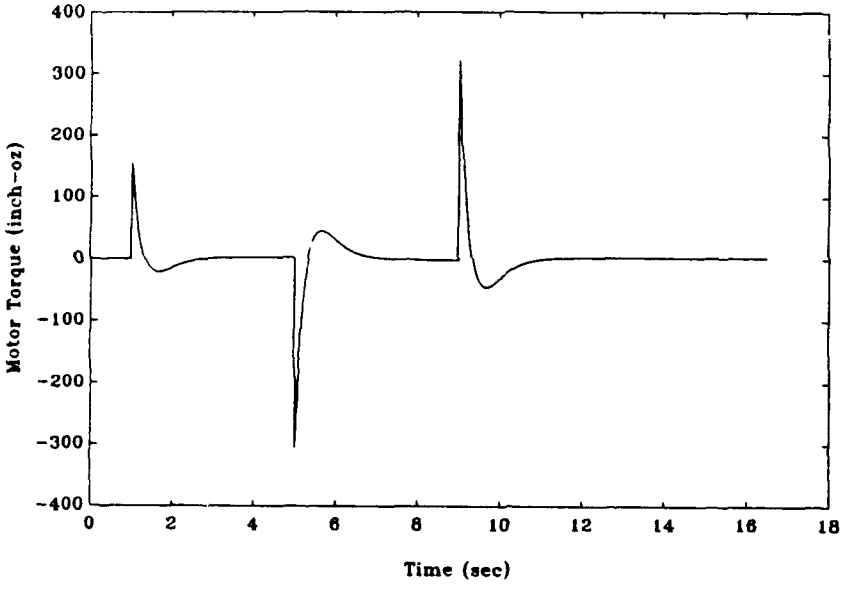

Figure 5-1 Motor Torque Required for Dahl Compensator

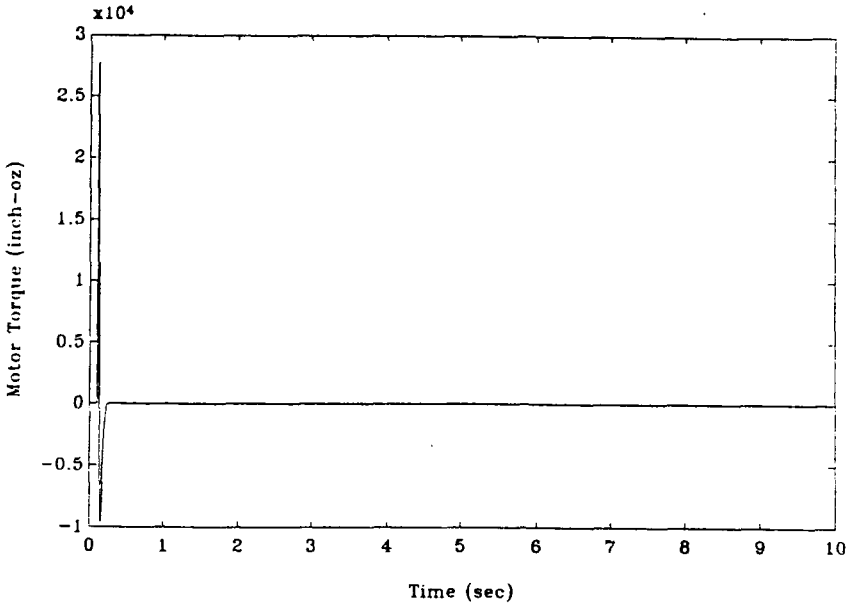

Figure 5-2 Motor Torque Required for Coulomb Compensator

much higher (around 1.75×10^4 inch-oz) than that required in the Dahl controller. The rates, $\dot{\Theta}$, for each compensator (with the large deflection input) are plotted in Figures 5-3 and 5-4. The required rate to meet the performance specification with the Coulomb controller is much greater than that for the Dahl controller. In fact, the combined torque and rate requirements of the Coulomb compensator would most probably be unachievable. The Coulomb compensator would certainly require a substantially larger motor than the Dahl compensator.

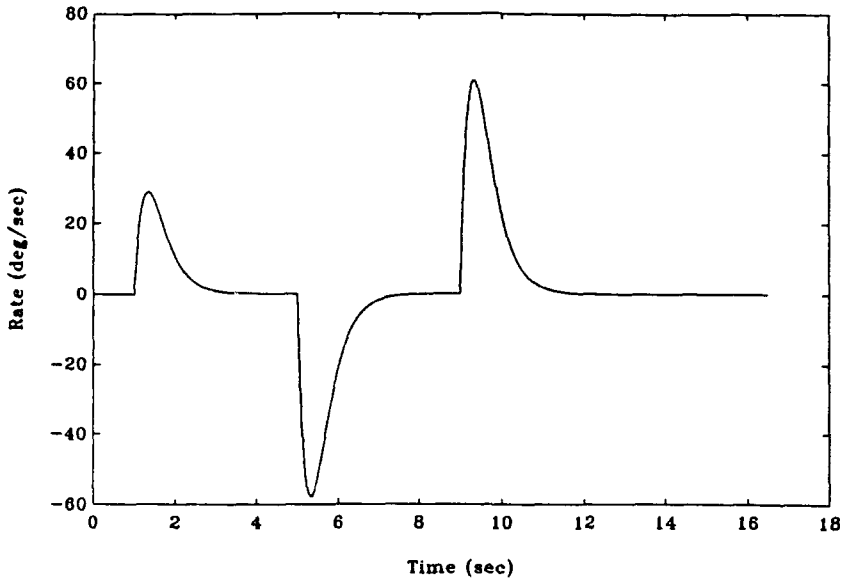

Figure 5-3 Gimbal Rate for Dahl Compensator

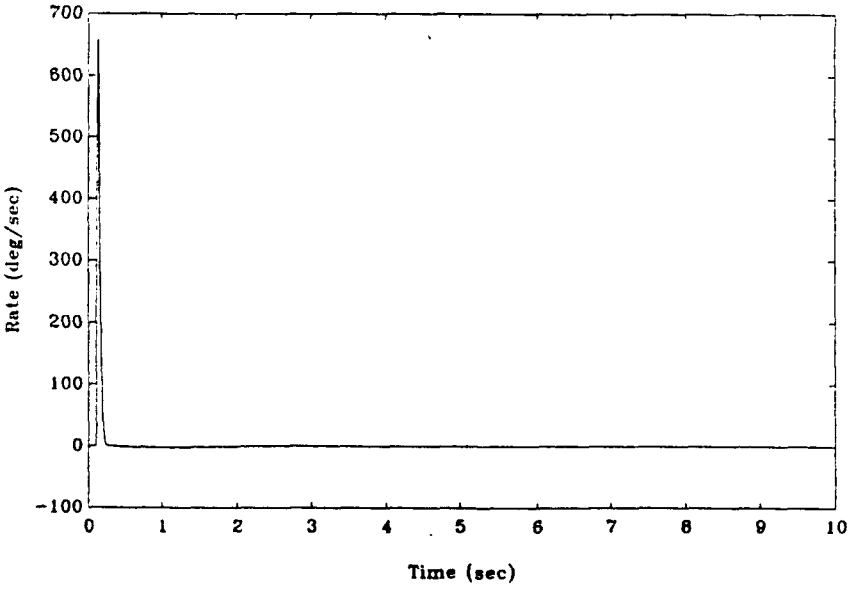

Figure 5-4 Gimbal Rate for Coulomb Compensator

5.1.2 Noise and Robustness. In Section 4.2 it was shown that the input measurement noise seemed to affect the Coulomb controller more so than the Dahl. This was also verified with other simulation runs that were not included for brevity. The Coulomb compensator performs its position regulation task adequateley, but its estimate of friction is very poor. This was demonstrated by Liebst (9) as well. Since the measurement noise is differentiated twice by the estimator and the friction model is too simplistic, poor friction estimation results. One way to improve the performance of the Coulomb contoller might be to measure acceleration with a low noise accelerometer and utilize it to drive the estimator as well.

The measurement noise did not affect the Dahl compensator in the same manner as it did the Coulomb controller. It was expected from the start of this research that the Dahl compensator would handle the noise better, since the extended Kalman filter has a higher fidelity friction model to use in its estimation, provided that the weights **Q** and **R** are set correctly. This brings up a major overlying issue concerning the Dahl compensator--its sensitivity to the weights. It is obvious from the simulation runs shown in Section 4.2, and from the numerous other runs made using the Dahl compensator, that it can be very sensitive to the values used for **Q** and **R**. It is presumed that, for this type of compensator to be used in a real system, a great deal of design effort must be expended toward a good understanding of the effects of the weights on a particular system. It is apparent that the system might have to be cycled

through a pre-mission start-up test. This was seen in the large deflection input case when the system was excited with an input within the compliance zone prior to seeing the large step. During this start-up phase, the system would be cycled through a predetermined commanded input to allow the Dahl friction model parameters to converge. **Q** and **R** might be varied to allow the system maximum flexibility in input deflection magnitudes or even scheduled and used for specific input deflection magnitude ranges. These would, however, be system design specific criteria that were not addressed here. With this in mind, a given system could be made to work well with measurement noise by changing the weights. In most cases this may also change the performance of the response characteristics slightly. This was shown in Figure 4-13d and 4-13e. By exciting the system within the Dahl compliance region and changing the weights slightly, it appears that the friction torque estimation is converging to the actual value. Although the position response performance did not appear to be degraded, the response time of the friction torque estimation did changed slightly. It is summized that there are weighting values that yield an optimal compromise between the noise robustness and specification perfomance.

Both compensators were checked for robustness to input deflection changes. Even though the Coulomb controller appeared to react well to a change in the input magnitude from large to small, the required motor torque was approximately nine times that which was required using the small

deflection input gains. Hence, it is very likely that some kind of gain scheduling may be required to allow for changes in input deflection magnitudes. The Dahl compensator, on the other hand, is very dependent on the particular extended Kalman filter weights chosen. As mentioned earlier, an actual system might require some kind of *weight scheduling* scheme or variable weighting methodology to allow for large changes in the magnitude of the input deflection. The Dahl compensator designs used in these simulations did not experience the large increase in required motor torque when changing the magnitude of the input. This is because the Dahl compensator designs used for both large and small input deflections had the same regulator poles.

5.2 Suggestions and Recommendations

Future research in this area should concentrate on issues concerning the weights **Q** and **R** for the extended Kalman filter and Dahl friction model controller. Even if this compensation method is too complicated and/or requires an unrealistic onboard computing capability for a real system control application, it could still prove to be valuable to bearing manufacturers. It would provide them with a means to test their bearings and measure the Dahl parameters σ and i.

Walrath claimed that the Dahl model exponential parameter, i, played no significant role in the model performance (3:719-720). If this is true, the number of friction parameters that must be estimated is reduced to just one, σ.

This would definitely make it easier on the controller and might give better results. Investigation of Walrath's claim would have to be carried out first.

Extended simulations were not run in this research due to the lengthy run times required for each simulation. Although the ProMatlab™ macros were very convenient and easy to use, there might be a more time efficient method that could be invoked. Possible alternatives might include the use of $MATRIX_x$ or direct Fortran programming. This would allow possible future researchers to run the simulations longer and possibly receive more insight into the phenomena that is occuring here.

A final observation is one made by Armstrong (1:51). To date, no investigation has been conducted to relate the micro-morphology of the contacting surfaces to the transition distance of the Dahl model. Understanding how the surface characteristics relate to the Dahl compliance region and friction parameters should certainly aid in the design and manufacture of bearings, as well as helping in the development of control system application designs.

Appenix A: ProMatlab™ M-Files for Coulomb Friction Model Compensation for a Single Axis Servo

A.1 Coulomb1.m

The following ProMatlab™ macro was used in simulations of the single axis servo system used in this research. This macro must be given the regulator and estimator gains, **k** and **l**, as well as a commanded input, **uc**, and the niose vector, **v**. It uses a time step of 0.01 seconds. Note also that a % represents a non-executable or comment line in ProMatlab™.

```
% This macro uses the basic system model with coulomb friction acting
% against the motor torque u.  Θc is the commanded input, theta command.
% The regulator and estimator gains k and l must be calculated previous
% to using this macro, and must be available in the Mat-file variable list.
%
%
%
%
%
%
%
%
%
%
%
%
%
%
%
%
%
%
%
%
%
%
xs=[];
```

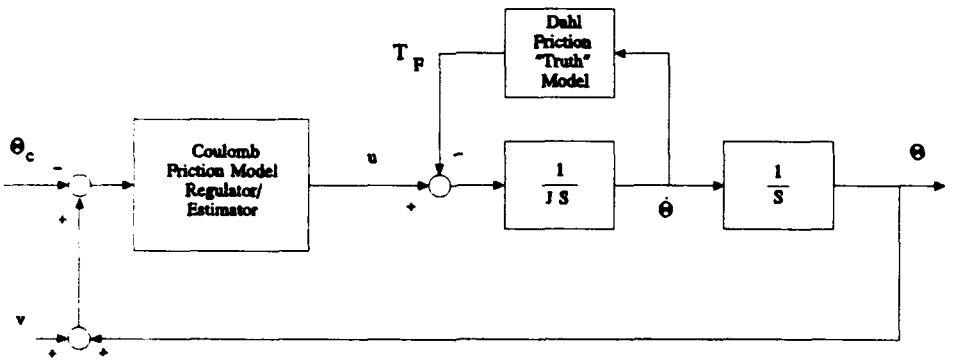

```
x=[0;0;0;sigma;ii];
x0=xinitial;p0=[0 0 0 0 0;0 0 0 0 0;0 0 0 0 0;0 0 0 0 0;0 0 0 0 0];
n=length(uc);nn=round(n/10);icount=0;iper=0;
ab=[0 1 0;0 0 -1/j;0 0 0]-[0;1/j;0]*k-l*[1 0 0];
[acomp,bcomp]=c2d(ab,l,.01);
xest=[0;0;0];
for i=1:n
z=x(1)+v(i);
xs=[xs;x' xest' u];
icount=icount+1;
if(icount==nn),icount=0;iper=iper+10;is=int2str(iper);...
disp([is,' % completed']),end
DF=x(4)*(1-x(3)/tc*sign(x(2)))^x(5);
u=-k*xest;
a=[0 1 0 0 0;0 0 -1/j 0 0;0 DF 0 0 0;0 0 0 0 0;0 0 0 0 0];
b=[0;1/j;0;0;0];
[ad,bd]=c2d(a,b,.01);
x=ad*x+bd*u;if(abs(x(3))>tc),x(3)=tc*sign(x(3));end
%*****************************************************************
%    Coulomb regulator/estimator compensation                    *
%*****************************************************************
xest=acomp*xest+bcomp*(z-uc(i));
end
```

A.2 Coulomb2.m

The following ProMatlab™ macro was also used for simulation of the Coulomb friction compensator. This version, howerver, has a time step of 0.001 seconds. This was done to allow the use of very fast estimator poles which would have saturated the discrete controller.

```
% This macro uses the basic system model with coulomb friction acting
% against the motor torque u.  θc is the commanded input, theta command.
% The regulator and estimator gains k and l must be calculated previous
% to using this macro, and must be available in the Mat-file variable list.
% This macro runs with a discrete time step of 0.001 seconds which means
% you have to use a large amount of points.  Use this version only when
% you have very fast estimator poles and you suspect that you're
% exceeding the bandwidth of the digitized controller.
```

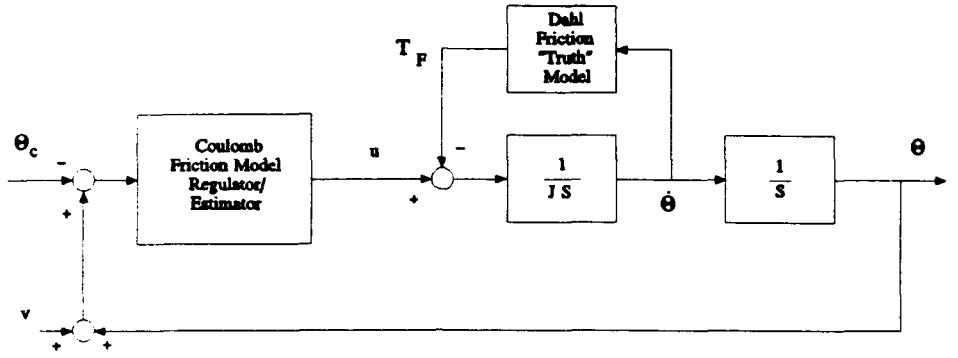


```
%
%
%
%
%
%
%
%
%
%
%
%
%
%
%
%
%
%
%
%
%
xs=[];
x=[0;0;0;sigma;ii];
x0=xinitial;p0=[0 0 0 0 0;0 0 0 0 0;0 0 0 0 0;0 0 0 0 0;0 0 0 0 0];
n=length(uc);nn=round(n/10);icount=0;iper=0;
ab=[0 1 0;0 0 -1/j;0 0 0]-[0;1/j;0]*k-1*[1 0 0];
[acomp,bcomp]=c2d(ab,1,.01);
xest=[0;0;0];
for i=1:n
z=x(1)+v(i);
xs=[xs;x' xest' u];
icount=icount+1;
if(icount==nn),icount=0;iper=iper+10;is=int2str(iper);...
disp([is,' % completed']),end
DF=x(4)*(1-x(3)/tc*sign(x(2)))^x(5);
u=-k*xest;
a=[0 1 0 0 0;0 0 -1/j 0 0;0 DF 0 0 0;0 0 0 0 0;0 0 0 0 0];
b=[0;1/j;0;0;0];
[ad,bd]=c2d(a,b,.001);
x=ad*x+bd*u;if(abs(x(3))>tc),x(3)=tc*sign(x(3));end
%*****************************************************************
%    Coulomb regulator/estimator compensation                    *
%*****************************************************************
xest=acomp*xest+bcomp*(z-uc(i));
end
```

Appendix B: ProMatlab™ M-File Simulating Single Axis Servo Using the Dahl Friction Compensator

```
% This is the basic system model with Dahl friction acting against
% the motor torque U. The input uc is the commanded position.
%
%
%
%
%
%
%
%
%
%
%
%
%
%
%
%
%
%
```

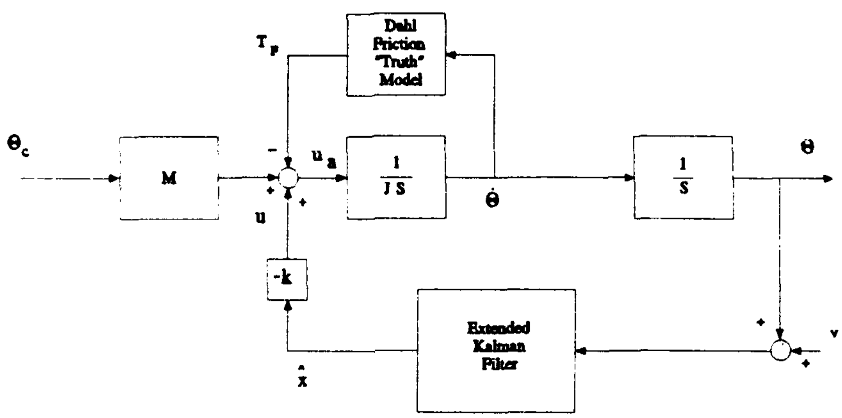


```
xs=[];
x=[0;0;0;sigma;ii];
x0=xinitial;p0=[0 0 0 0 0;0 0 0 0 0;0 0 0 0 0;0 0 0 0 0;0 0 0 0 0];
n=length(uc);nn=round(n/10);icount=0;iper=0;
ksave=[];
for i=1:n
z=x(1)+v(i);
xs=[xs;x' x0' u];
icount=icount+1;
if(icount==nn),icount=0;iper=iper+10;is=int2str(iper);...
disp([is,' % completed']),end
DF=x(4)*(1-x(3)/tc*sign(x(2)))^x(5);
ua=-kk*x0(1:3)+M*uc(i);
a=[0 1 0 0 0;0 0 -1/j 0 0;0 DF 0 0 0;0 0 0 0 0;0 0 0 0 0];
b=[0;1/j;0;0;0];
[ad,bd]=c2d(a,b,.01);
x=ad*x+bd*ua;if(abs(x(3))>tc),x(3)=tc*sign(x(3));end
```

```
% ***************************************************************
%   Extended Kalman Filter estimation                          *
% ***************************************************************
xestk=x0;pk=p0;
% **********************************
%   setting up F=df/dx|x=xest      *
% **********************************
qlog=1-xestk(3)/tc*sign(xestk(2));
df1=[0;0;0;0;0];
df2=[1;0;0;0;0];
if(qlog~=0)
df2=[1;0;xestk(4)*(qlog)^xestk(5);0;0];
end
df3=[0;1/j;0;0;0];
if(qlog~=0)
df3=[0;-1/j;xestk(4)*xestk(5)*(qlog)^(xestk(5)-1)*...
xestk(2)*(-1/tc)*sign(xestk(2));0;0];
end
df4=[0;0;0;0;0];
if(qlog~=0)
df4=[0;0;(qlog)^xestk(5)*xestk(2);0;0];
end
df5=[0;0;0;0;0];
if(qlog~=0)
df5=[0;0;xestk(4)*(qlog)^xestk(5)*xestk(2)*...
log(qlog);0;0];
end
F=[df1 df2 df3 df4 df5];
% **********************************
DFest=0;
if(qlog~=0)
DFest=xestk(4)*(1-xestk(3)/tc*sign(xestk(2)))^xestk(5);
end
pdot=F*pk+pk*F'+G*Q*G';
xestdot=[xestk(2);1/j*(u-xestk(3));DFest*xestk(2);0;0];
xestkp1uc=xestk+xestdot*delt;
pkp1uc=pk+pdot*delt;
H=[1 0 0 0 0];
k=pkp1uc*H'*inv(H*pkp1uc*H'+r);
ksave=[ksave;k'];
xestcor=xestkp1uc+k*(z-xestkp1uc(1));if(abs(xestcor(3))>tc),...
xestcor(3)=tc*sign(xestcor(3));end
if(xestcor(4)<1),xestcor(4)=0;end
```

```
pkcor=pkp1uc-k*H*pkp1uc;
x0=xestcor;p0=pkcor;
%*************************************************
end
%*************************************************
end
```

Bibliography

1. Armstrong, Brian S. R. *Dynamics for Robot Control: Friction Modeling and Ensuring Excitation During Parameter Identification.* PhD dissertation. Stanford University, Palo Alto, Calif., 1988.

2. Himmel, Lewis A. et al. "Examination of Adaptive Control-based Approach to Friction Compensation in Space Craft Gimbal Control Systems," *Proceedings of the 24th Conference on Decision and Control.* 642-644. New York: IEEE Press, 1985.

3. Walrath, Craig D. "Adaptive Bearing Friction Compensation Based on Recent Knowledge of Dynamic Friction," *Automatica, 20*: 717-727 (July 1984).

4. Shames, Irving H. *Engineering Mechanics: Statics and Dynamics.* New Jersey: Prentice-Hall, inc., 1980.

5. Dahl, P. R. "Measurements of Solid Friction Parameters of Ball Bearings," *Sixth Annual Symposium on Incremental Motion Control Systems and Devices Proceedings.* University of Illinois, 1977.

6. Culver, Robert C. *Evaluation of Concepts for a Laser Acquisition and Tracking System*, 1 June 1972 - 1 April 1973. Contract Number F33615-72-C-2053. Boulder, Colo.: Ball Brothers Research Corp., May 1973.

7. Dahl, P. R. "Solid Friction Damping of Spacecraft Ocsillation," *AIAA Guidance and Control Conference Proceedings*, Boston, Mass., 1975.

8. Franklin, Gene F. et al. *Feedback of Dynamic Control Systems.* Massachusetts: Addison-Wesley, 1986.

9. Liebst, Brad S. and Verbanets, W. "Compact, High-Accuracy, Inductosyn Based Gimbal Control System," *Proceedings of the 1991 SPIE OE/Aerospace Sensing Conference*, Orlando, Florida, April 1991.

10. Kautsk, J. and Nichols, N. K. *Robust Eigenstructure Assignment in State Feedback Control.* Numerical Analysis Report NA/2/83, School of Mathematics, Flinders U., Bedford Park, S.A. 5042, Australia.

11. Maybeck, Peter S. *Stochastic Models, Estimation and Control*, vol 2. New York: Academic Press, 1982.

REPORT DOCUMENTATION PAGE

Form Approved
OMB No 0704-0188

1. AGENCY USE ONLY (Leave blank)	2. REPORT DATE	3. REPORT TYPE AND DATES COVERED
	December 1991	Master's Thesis

4. TITLE AND SUBTITLE

Comparison of Pointing Control Systems Utilizing Dahl and Coulomb Friction Model Compensation

5. FUNDING NUMBERS

6. AUTHOR(S)

Whitney J. Hulett, Captain, USAF

7. PERFORMING ORGANIZATION NAME(S) AND ADDRESS(ES)

Air Force Institute of Technology, WPAFB OH 45433-6583

8. PERFORMING ORGANIZATION REPORT NUMBER

AFIT/GAE/ENY/91D-16

9. SPONSORING / MONITORING AGENCY NAME(S) AND ADDRESS(ES)

10. SPONSORING / MONITORING AGENCY REPORT NUMBER

11. SUPPLEMENTARY NOTES

12a. DISTRIBUTION / AVAILABILITY STATEMENT

Approved for public release; distribution unlimited

12b. DISTRIBUTION CODE

13. ABSTRACT *(Maximum 200 words)*

Bearing friction can be accurately modeled using the Coulomb friction model, provided the bearing is running. In an application where the bearing is rotated only a very small amount, the bearing does not actually rotate. Instead, the bearing undergoes *plastic* deformation. A nonlinear friction model was developed by P. R. Dahl of the Aerospace Corporation in the late sixties which addresses this region of placticity or compliance zone. Two friction compensation schemes for a single axis position servomechanism were developed and compared in this study. The first compensator was an integral control regulator/estimator which used the Coulomb friction model. The second, more complicated compensator, was an extended Kalman filter (EKF) design which used the Dahl friction model. The compensator designs were simulated using ProMatlab™. Comparisons were made of the time response characteristics to determine if any increases in performance were worth the added complexity of the Dahl model EKF controller.

14. SUBJECT TERMS	15. NUMBER OF PAGES
Friction, Dahl Friction, Coulomb Friction, Nonlinear Friction Friction Compensation, Adaptive Control	99
	16. PRICE CODE

17. SECURITY CLASSIFICATION OF REPORT	18. SECURITY CLASSIFICATION OF THIS PAGE	19. SECURITY CLASSIFICATION OF ABSTRACT	20. LIMITATION OF ABSTRACT
Unclassified	Unclassified	Unclassified	UL